1986

Dead reckoning control of an automated guided vehicle /

Herbert W. Conover III
Lehigh University

DEAD RECKONING CONTROL OF AN AUTOMATED GUIDED VEHICLE

By

HERBERT W. CONOVER III

A Thesis

Presented to the Graduate Committee

of Lehigh University

in Candidacy for the Degree of

Master of Science

Mechanical Engineering

Lehigh University

1986

This thesis is accepted and approved in partial fulfillment of the requirements for the degree of Master of Science.

August 4, 1986
(Date)

Russell E. Benner
Professor in Charge

F. Erdogan
Chairman of Department

ACKNOWLEDGEMENTS

The author would like to thank the following people. Dr. R. E. Benner for his guidance and insight throughout the research.

Dr. M. P. Groover for his support as the director of the research project. Dr. S. H. Johnson and Dr. W. E. Schiesser for their many discussions and suggestions.

Thanks also goes to the Ben Franklin Organization and SI Handling Company for their financial support.

The author would also like to especially thank his parents, Charlotte and Herbert W. Conover Jr. , for their love and support. Special thanks also goes to the authors constant and enduring companion Miss Emilie A. Schreffler.

Finally, thanks are extended to Mark Behringer, Mark Cortazzo, Blaine Taylor, Ronald Koontz, and Raymond Vogt, for their friendship and support.

TABLE OF CONTENTS

LIST OF FIGURES

ABSTRACT

This thesis presents the controller algorithms and equations necessary to guide an automated guided vehicle (AGV). Current AGV controllers make use of external position feedback to guide the vehicle. Dead reckoning control does not use external position feedback, but internally calculates the position of the AGV and periodically updates the vehicle's absolute position.

The equations necessary to guide the vehicle along a series of straight line segments are presented. Separate simulations of the straight line controller, the turning controller, and the complete controller are presented.

Each controller was found to perform satisfactorily. The complete controller can be enhanced by eliminating the straight line controller's offset error.

INTRODUCTION

An automated or automatic guided vehicle system (AGVS) is a material handling system that uses independently operated, self-propelled vehicles which are guided along defined pathways. Automated guided vehicle systems are used in manufacturing systems, storage systems, and traditional materials handling applications.

Various uses and forms of the automated guided vehicle (AGV) exist. The vehicles are used to form driverless trains, where the AGV pulls one or more trailers. Automated guided vehicles are also used as pallet trucks, which carry loads up to 6000 lbs. Most vehicles are designed as tricycles and are driven by an electric motor mounted to the front wheel steering assembly.

Several guidance systems are currently used with AGVs. The term guidance system refers to the method by which the AGVs pathways are defined and the vehicle control system that follows the pathways [1]. The two principal methods now in use are: guide wires imbedded in the floor, and optical methods which sense flourescent lines painted on the floor. Both methods follow physically permanent paths and utilize position feedback to stay on course.

A third type of guidance system is dead reckoning control. Dead reckoning follows an internally memorized path and does not use external position feedback to follow a given path. Straight line path segments, which define the desired trajectory, are stored in

the vehicle's on-board memory. A microprocessor computes the vehicle's position and orientation using rear wheel shaft encoders; the shaft encoders supply the angular position of each rear wheel. Control algorithms are used with the encoder data to follow the successive straight line segments. Dead reckoning control can be enhanced by periodically updating the vehicle's absolute position. Absolute position update is a prerequisite since error may be present in the encoder output.

The objective of the research was to design, develop, and simulate the control algorithms necessary to implement dead reckoning control. Two separate controllers were developed; a straight line controller to keep the AGV moving along a straight line segment, and a turn controller which delivers the AGV from one straight line segment to the next. Complete dead reckoning control was achieved by linking together the two separate controllers.

STRAIGHT LINE CONTROLLER

The straight line controller maintains the AGV on a straight line segment. Various conditions cause the AGV to deviate from a desired segment. Deformation of the vehicle's tire material causes the AGV to move in unpredicted directions. Wheel deformation occurs due to loads carried by the vehicle, and the centrifugal force experienced during turns. The vehicle's physical configuration also creates straight line deviation. Inaccuracies in the mounting of the rear wheels, as well as error in the orientation of the front steering wheel cause straight line tracking error.

The straight line controller models the AGV as a tricycle. A detailed description of the vehicle model is found in Appendix A. The actual physical job of the straight line controller is to minimize the position error ε_d, and orientation error ε_θ. The controller minimizes ε_d and ε_θ by making adjustments in the vehicle's steering wheel angle α. When the position and orientation errors are equal to zero, the vehicle is moving along a prescribed straight line segment. A detailed description of ε_d and ε_θ is found in Appendix B.

The straight line controller is a single output, dual input controller. The two outputs are the $\varepsilon_d(s)$ and $\varepsilon_\theta(s)$, while the input is $\alpha(s)$. The transfer functions of the system's plants, $G_1(s)$

and $G_2(s)$ are derived in Appendix C. The controller is proportional only, with both $\varepsilon_d(s)$ and $\varepsilon_\theta(s)$ feedback. The manipulated variable $C_\alpha(s)$ is formed by summing the quantities $k_1(\varepsilon_{d(s)}^{set} - \varepsilon_{d(s)})$ and $k_2(\varepsilon_{\theta(s)}^{set} - \varepsilon_{\theta(s)})$. The manipulated variable is written:

$$C_{\alpha(s)} = k_1(\varepsilon_{d(s)}^{set} - \varepsilon_{d(s)}) + k_2(\varepsilon_{\theta(s)}^{set} - \varepsilon_{\theta(s)}) . \quad (1)$$

The steering angle $\alpha(s)$ is formed by multiplying the manipulated variable by a first order approximation of the steering assembly. The relationship between $\alpha(s)$ and $C_{\alpha(s)}$ is written:

$$\frac{\alpha(s)}{C_\alpha(s)} = \frac{1}{1 + \tau s} = G_{v(s)} , \quad (2)$$

where τ is the steering assemblies time constant, and $G_{v(s)}$ is used for notation. The controller's setpoints $\varepsilon_{d(s)}^{set}$ and $\varepsilon_{\theta(s)}^{set}$ are set equal to zero at all times. The block diagram of the straight line controller is seen in Figure 1.

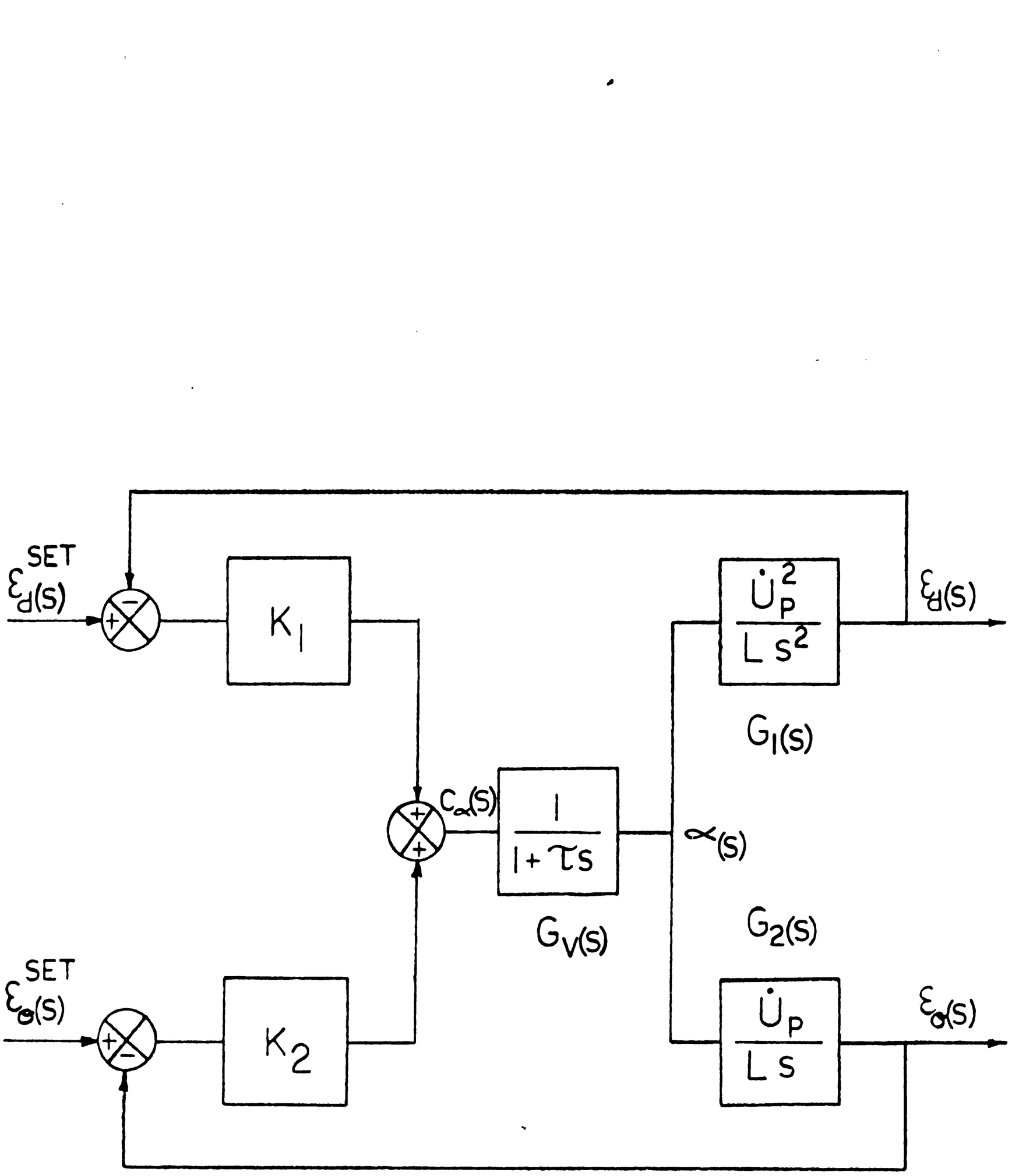

Figure 1: Block diagram of straight line controller

Block diagram reduction of Figure 1 leads to a third-order, linear, differential equation which describes the vehicle's position error ε_d as a function of time. The equation is:

$$\frac{\tau L}{U_p^2}\dddot{\varepsilon}_d + \frac{L}{U_p^2}\ddot{\varepsilon}_d + \frac{k_2}{U_p}\dot{\varepsilon}_d + k_1\varepsilon_d = 0 \qquad [2], \quad (3)$$

where the dots represent differentiation with respect to time. The third order equation was reduced to a system of three coupled, first order equations. The three equation system was used for simulation. The controller gains, k_1 and k_2, were calculated with a root contour analysis. A detailed derivation of the straight line controller governing equations and the root contour gain calculations are found in Appendix C.

Turn Control

The turn controller is an algorithm which appropriately modifies the vehicle's steering wheel angle to negotiate a given turn. The negotiation of a turn consists of moving from the S_k path segment, to the S_{k+1} path segment. The vehicle's point p travels along a smooth, circular arc when moving from the S_k segment to the S_{k+1} segment. A description of the segment identification convention and equations are found in Appendix B.

Three first order differential equations are used to describe the vehicle's position. The position coordinates are orientation θ, x-axis position x, and y-axis position y. The position variables θ, x, and y are measured relative to a fixed reference system. The three governing equations are:

$$\frac{d\theta}{dt} = \frac{\dot{u}_Q}{L} \sin(\alpha) \quad , \qquad (4)$$

$$\frac{dx}{dt} = \dot{u}_Q \cos(\alpha)\cos(\theta) \quad , \qquad (5)$$

$$\frac{dy}{dt} = \dot{u}_Q \cos(\alpha)\sin(\theta) \quad . \qquad (6)$$

Equations 4, 5, and 6 are derived in Appendix D.

The vehicle's position is also measured relative to coordinate systems other than the fixed reference system. The position of the vehicle is measured relative to the current path segment, as well as relative to the next segment. Diagrams of the coordinate systems attached to the current and the next path segment are given in Appendix B.

The quantity MT is measured relative to the current path segment, and is used to signal the switch from the straight line controller to the turn controller. The quantity MT is the distance from the end of the current path segment to the point p on the vehicle. When the vehicle moves within a critical MT value, MTCRT, the turn algorithm begins. MT is given by the equation:

$$MT = \left| \frac{\hat{\epsilon}_d}{\sin(\hat{\epsilon}_\theta)} \right| . \qquad (7)$$

In order to negotiate a given turn, two important quantities must be calculated: ANG, the theoretical steering angle required to complete the given turn, and TT, the theoretical amount of time to complete the turn. A turn is complete when the vehicle's point p intersects the S_{k+1} segment. The equations for ANG and TT are:

$$ANG = \tan^{-1}\left[\frac{L(1-\cos\hat{\epsilon}_\theta)}{\hat{\epsilon}_d - \dot{u}_p \tau_D \sin\hat{\epsilon}_\theta}\right] , \qquad (8)$$

and

$$TT = \frac{\hat{\varepsilon}_\theta(\hat{\varepsilon}_d - \dot{u}_p \tau_D \sin\hat{\varepsilon}_\theta)}{\dot{u}_p(1-\cos\hat{\varepsilon}_\theta)} . \qquad (9)$$

The development of equations 8 and 9 are found in Appendix D.

The AGV steering assembly is modeled using a simple linear ramp model. To negotiate a given turn, the steering assembly is ramped to ANG, held constant for a prescribed amount of time, and finally ramped down to a steering angle of zero. The variable τ_s, or the time required for the steering assembly to reach a steering angle of ninety degrees, characterizes the steering assembly. The steering assembly is assumed incapable of reaching a steering angle greater than ninety degrees. The equation yielding the amount of time required for the steering assembly to reach the value ANG is:

$$T1 = \frac{ANG\tau_s}{1.5708} . \qquad (10)$$

A more complete description of the steerring assembly model is found in Appendix D.

Modification of the turn algorithm is required in order to avoid inaccurate turns. Turn inaccuracy is developed because the steering assembly does not instantaneously reach the prescribed theoretical steering angle, ANG. The two problems which occur are

turn overshoot and turn orientation error. Turn overshoot leaves the vehicle's point p with an ε_d position error, while turn orientation error leaves the vehicle with an orientation error, ε_θ.

Turn overshoot is eradicated through the parameter, τ_D. The quantity τ_D is a time lead which defines the point from which ANG and TT are calculated. The larger τ_D, the farther along the S_k segment ANG and TT are calculated. Setting τ_D greater than zero yields larger values of ANG and smaller values of TT. Essentially, the vehicle begins to turn at some time earlier than is theoretically required. The τ_D value is proportional to the vehicle's velocity and the angular error between the vehicle and the next path segment:

$$\tau_D = k\, \dot{u}_p \hat{\varepsilon}_\theta \quad . \qquad (11)$$

The proportionality constant k is set through simulation.

Turn orientation error is remedied by holding the steering assembly at the value ANG for a time greater than is theoretically required. The quantity T2, or the theoretical amount of time which the assembly is held at ANG, is essentially increased by the amount of time taken during the assemblies ramp up and ramp down. The new T2 is calculated with the equation:

$$T2 = T2 + CON\ T1 \quad , \qquad (12)$$

where T1 is the time required to ramp up to or down from ANG, and CON is set through simulation.

COMPLETE CONTROL

The complete control of the vehicle is achieved through "connecting" the straight line and turning controllers. The complete controller assigns the steering wheel angle according to the vehicle's position. The angle is calculated using either the straight line or turning controller. The complete control algorithm flow chart is seen in Figure 2.

A detailed discussion of the complete control algorithm follows.

The algorithm begins with the initialization of the following:

- Physical parameters of the vehicle
- Straight line controller gains
- Critical MT value
- Dependent variables D1 through D6
- Segments which make up the desired path
- Segment lengths and orientations
- Position variables x*, y*, and $\hat{\varepsilon}_d$.

After initialization, the vehicle's position is calculated. The following quantities are calculated:

$-\dot{u}_p, \varepsilon_\theta, \hat{\varepsilon}_\theta, MT, x^*, y^*, \hat{\varepsilon}_d, \hat{y}$.

The controller next asks if the vehicle's MT value is less than or equal to the critical MT value. If the MT value is not less than the critical value, the controller uses the straight line

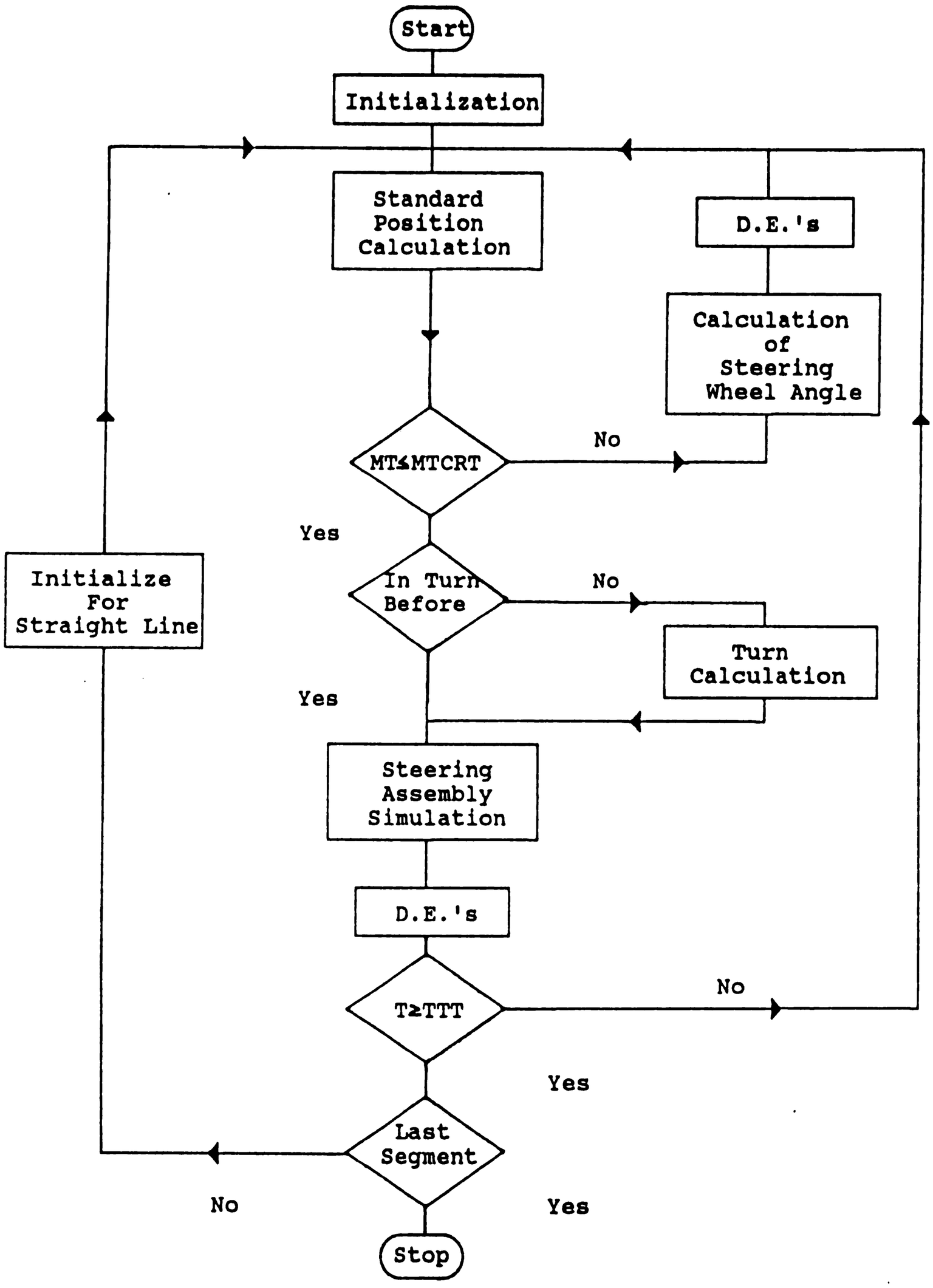

Figure 2: Flow chart of complete control algorithm

controller. On the other hand, if the MT value is less than the critical value, the complete controller uses the turn controller.

Consider the value of MT being greater than the critical value. The complete controller first calculates the steering wheel angle according to the straight line controller and then integrates all six dependent variables ($\varepsilon_d, \dot{\varepsilon}_d, \ddot{\varepsilon}_d, \theta, x, y$). The complete controller moves forward in time, calculates the vehicle's new position, and asks if MT is less than or equal the critical value.

Now consider the value of MT to be less than the critical value. The complete controller uses the turn controller to guide the vehicle. The complete controller asks if turn initialization is required. If turn initialization is required, the complete controller does the following:

- Calculates the angular difference between the present path segment and the next path segment (calculation of turn orientation).

- Calculates τ_D according to how sharp the desired turn is. Calculates both the theoretical steering wheel angle to complete the desired turn, ANG and the theoretical time to complete the turn, TT.

- Calculates the modified turning times according to how long the steering wheel angle is to be held constant through the turn. The absolute value of time at the end of the turn is calculated and called TTT.

The turn is now completely initialized and ready to begin.

The complete controller begins the turn control by choosing the steering wheel angle from the steering simulator. The steering simulator is responsible for ramping the steering angle up and down during the turn. After the steering angle is assigned, the straight line controller integrates the dependent variables θ, x, and y.

Next, the straight line controller asks if time is greater than or equal to the absolute time at the end of the turn, TTT. If time is less than TTT, the complete controller moves forward in time, calculates the vehicle's new position, and continues moving around the turn. If time is greater than or equal to TTT, the controller makes certain it is not moving to the last segment and then reinitializes for the straight line controller. To reinitialize the following variables are calculated:

$$- \varepsilon_d,\ \dot{\varepsilon}_d,\ \ddot{\varepsilon}_d,\ \varepsilon_\theta,\ \hat{\varepsilon}_\theta,\ x^*,\ y^*,\ MT.$$

Note that the calculations required to initialize ε_d must be done relative to the next path segment. This is implemented by numbering the segments, and incrementing the current segment value when straight line initialization occurs. The complete controller begins again at the top of the algorithm.

Finally, if the last segment is the current segment, the controller stops. If the vehicle's desired path contains n segments, an n+1 or dummy segment is utilized.

VEHICLE DYNAMICS

Vehicle dynamics can be included in the guidance control algorithms to more accurately predict the position and orientation of the vehicle during dead reckoning. The present simulation does not include the vehicle's rolling dynamics, but can be included using the equations given below.

The major cause of dynamic tracking error is the centrifugal force experienced by the vehicle while moving through a turn. The centrifugal force causes the wheel material to deform. The wheel deformation causes the vehicle to follow a path which is not predicted by the geometric position equations. The angle between the geometric path and the actual path is known as the slip angle. Slip angles can be experimentally determined for various vehicle configurations and turns [3].

The kinematic model used with the vehicle is shown in Figure 3. The model is two dimensional with all motion existing in the xy-plane. A better dynamic model would consider the vehicle's center of mass in another plane and different wheel loads. During a turn the vehicle of mass M experiences a centrifugal force C, and each wheel experiences a side force. The side forces on the left, right, and front wheels are denoted as S_ℓ, S_r, and S_f respectively. The vehicle's front wheel provides a tractive force T which causes the

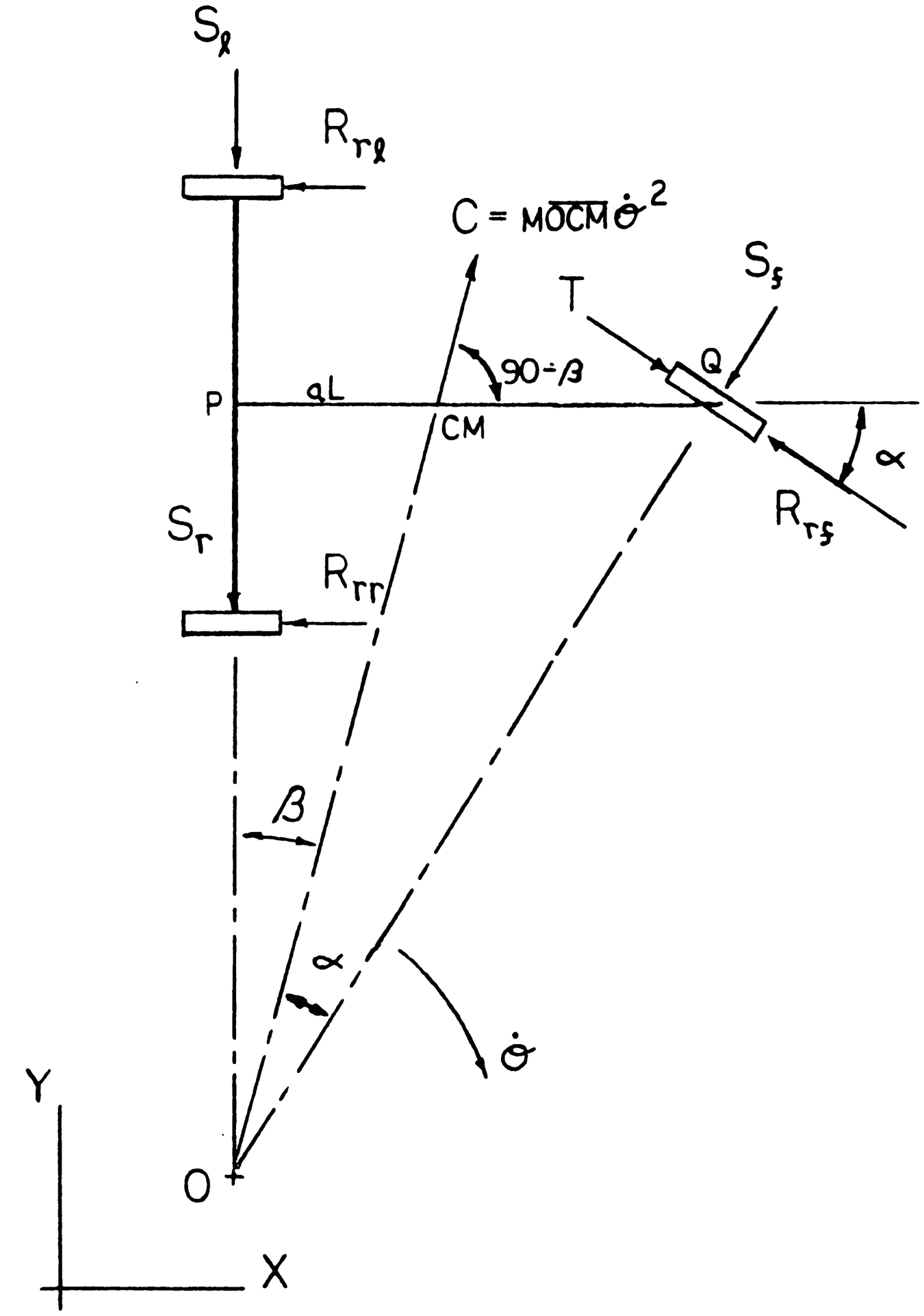

Figure 3: Kinematic model of the vehicle

vehicle's motion. Each wheel also experiences a rolling resistance force. The rolling resistance forces on the left, right, and front wheels are denoted as $R_{r\ell}$, R_{rr}, and R_{rf} respectively.

Three equations were used to determine the wheel side forces. Given the vehicle configuration, steering wheel angle, and rolling resistance values, $S_\ell+S_r$, T, and S_f are determined using:

$$(S_\ell+S_r) = \frac{(1-a)C}{\sqrt{a^2\tan^2\alpha+1}} + \frac{E}{2}(R_{rr}-R_{r\ell}) , \qquad (13)$$

$$T = R_{rf} + \frac{1}{2\cos\alpha}\left[(R_{r\ell}+R_{rr}) - \frac{aC\tan\alpha}{\sqrt{a^2\tan^2\alpha+1}}\right] + \frac{1}{2\sin\alpha}\left[\frac{E}{2L}(R_{rr}-R_{r\ell}) + \frac{aC}{\sqrt{a^2\tan^2\alpha+1}}\right] , \qquad (14)$$

$$S_f = \frac{1}{2\cos\alpha}\left[\frac{aC\tan\alpha}{\sqrt{a^2\tan^2\alpha+1}} - (R_{r\ell}+R_{rr})\right] + \frac{1}{2\sin\alpha}\left[\frac{E}{2L}(R_{rr}-R_{r\ell}) + \frac{aC}{\sqrt{a^2\tan^2\alpha+1}}\right] , \qquad (15)$$

See Appendix E for development of equations 13, 14, and 15.

Once the side forces are calculated, the slip angles can be obtained from experimental data which relates side force and slip angle.

When the vehicle moves through a turn, it geometrically or theoretically rotates about a point 0, and actually rotates about a point 0'. The shifting of the center of rotation from 0 to 0' is due to wheel slip, or the slip angles. Figure 4 shows the vehicle moving through a turn with the shifted center of rotation. Note that in the following dynamics equations the side forces S_ℓ and S_r are assumed to act along the y-axis, thus both γ_p and γ_r are zero and the shifted centrifugal force C' becomes C. With this assumption the vehicle's slip can be described using γ_p and γ_f. The new center of rotation is described using:

$$\overline{o'cm} = L\{(1-a)^2 + \frac{\cos^2\gamma_p}{\sin^2(\alpha+\gamma_p-\gamma_f)} - 2(1-a)\frac{\cos\gamma_p \sin(\alpha-\gamma_f)}{\sin(\alpha+\gamma_p-\gamma_f)}\}^{1/2}. \quad (16)$$

The angle ψ, which describes the orientation of the centrifugal force, is given by:

$$\psi = \sin^{-1}\left[\frac{\cos\gamma_p \cos(\alpha-\gamma_f)}{\sin(\alpha+\gamma_p-\gamma_f)\ R}\right], \quad (17)$$

where R is given by equation E-21.

See Appendix E for the development of equations 16 and 17.

Finally, equations 13, 14, and 15 are rewritten in terms of ψ:

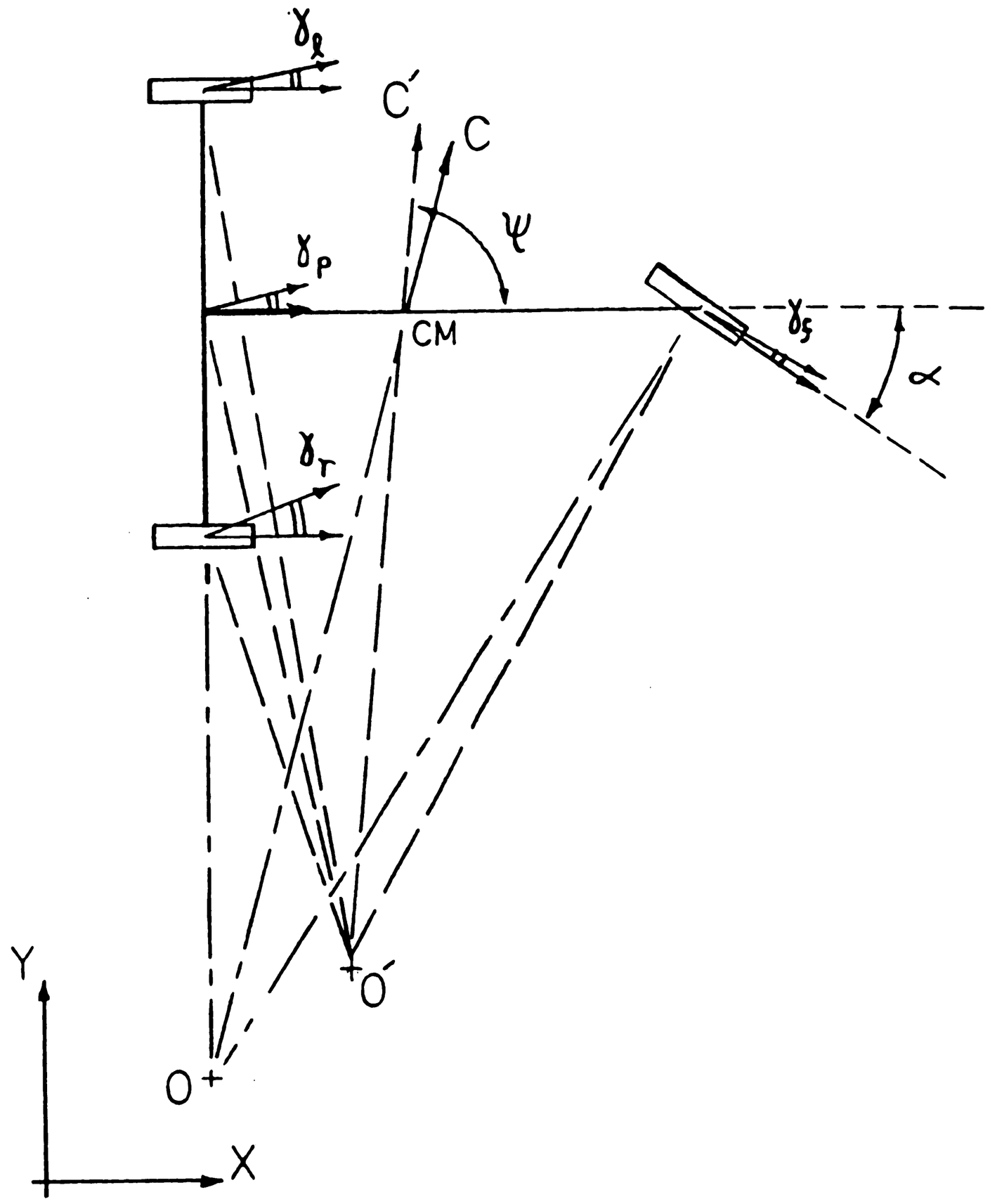

Figure 4: Shifted center of rotation due to slip

$$(S_\ell + S_r) = (1-a)C\sin\psi + \frac{E}{2L}(R_{rr} - R_{r\ell}) \quad , \qquad (18)$$

$$T = R_{rf} + \frac{(R_{r\ell} + R_{rr}) - C\cos\psi}{2\cos\alpha} + \frac{aC\sin\psi + \frac{E}{2L}(R_{rr} - R_{r\ell})}{2\sin\alpha} \quad , \qquad (19)$$

$$S_f = \frac{aC\sin\psi + \frac{E}{2L}(R_{rr} - R_{r\ell})}{2\sin\alpha} - \frac{(R_{r\ell} + R_{rr}) - C\cos\psi}{2\cos\alpha} \quad . \qquad (20)$$

See Appendix E for the development of equations 18, 19, 20.

The algorithm to calculate the slip angles with dynamic effects is:

A. Assume γ_p is due to $S_\ell + S_r$. Use equations 13 and 15 to calculate $S_\ell + S_r$ and S_f.

B. Obtain γ_p and γ_f from experimental data.

C. Calculate $\overline{o'cm}$ using equation 16 and the slip angle values found in B.

D. Calculate ψ using equation 17.

E. Calculate C using: $C = m\overline{o'cm}\theta^2$.

F. Calculate $S_\ell + S_r$, and S_f using equations 18 and 20.

G. Obtain the iterated γ_p and γ_f from experimental data.

RESULTS

The major results of the research are the development of the complete control algorithm and the computer simulation of the algorithm.

The programming of the complete control algorithm was accomplished by first separately simulating the straight line and turn controllers. The straight line simulation shows the vehicle returning to a straight line segment after being assigned an initial position error, orientation error, and steering wheel angle. The turn simulation shows the vehicle completing a desired turn. The straight line program is used to set the straight line controller gains, k_1 and k_2, while the turn program is used to set τ_D and CON. After k_1, k_2, τ_D, and CON have been set, the complete simulation program is run and the graphical output evaluated.

The following is a discussion of the graphical results of the straight line, turn, and complete controllers. Each simulation used the following vehicle configuration:

$\dot{u}_Q$ = 2.0 ft/s,

L = 2.5 ft,

E = 2.83 ft,

τ = .7,

τ_s = 1.0 .

The discussion is in terms of each figure.

The straight line and turn simulations picture the vehicle's tricycular frame. Straight line segments are identified in the turn and complete simulations by the sharp angle defined when two segments are joined.

STRAIGHT LINE CONTROLLER RESULTS:

Figure 5: Initial position error of -.5 ft. The vehicle moves smoothly back to the straight line segment within 10.0 ft in the y direction. The controller gains were k_1=.2 and k_2=1.25.

The speed with which the vehicle returns to the straight line segment can be decreased or increased by varying the k_1 gain.

Figure 6: Initial position error of -.5 ft. The vehicle moves smoothly back to the straight line segment within 20.0 ft in the y-direction. The higher settling time was achieved by setting the controller gains at k_1=.1, and k_2=1.25.

Figure 7: Initial position error of -.5 ft. The vehicle moves back to the straight line segment with overshoot. The vehicle does not completely move on to the straight line segment until 25.0 ft. of y-direction travel. The overshoot was achieved by setting the controller gains at k_1=.4, and k_2=1.25. Straight line control with overshoot could be desired in complete control.

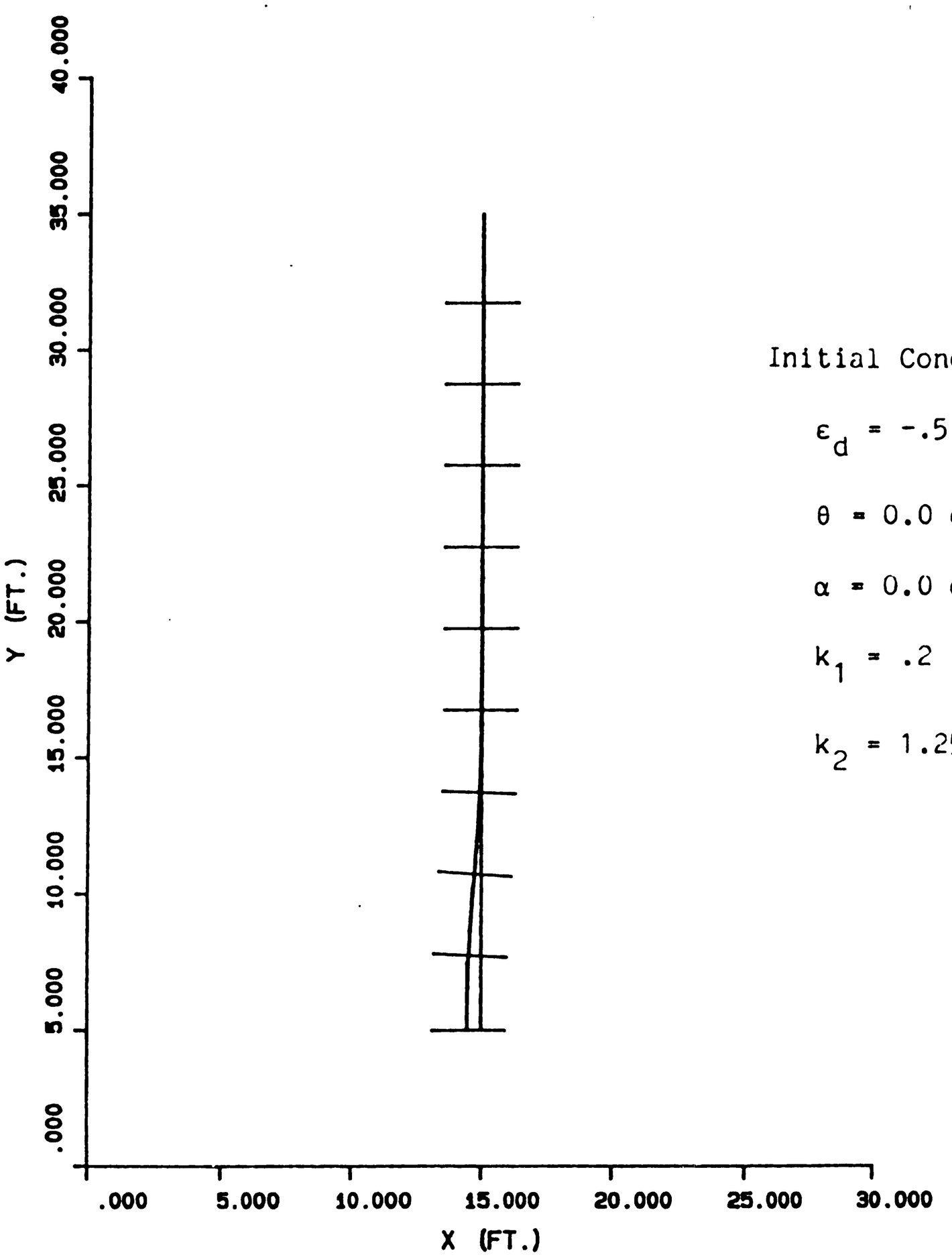

STRAIGHT LINE CONTROL

Figure 5: Straight line simulation (1)

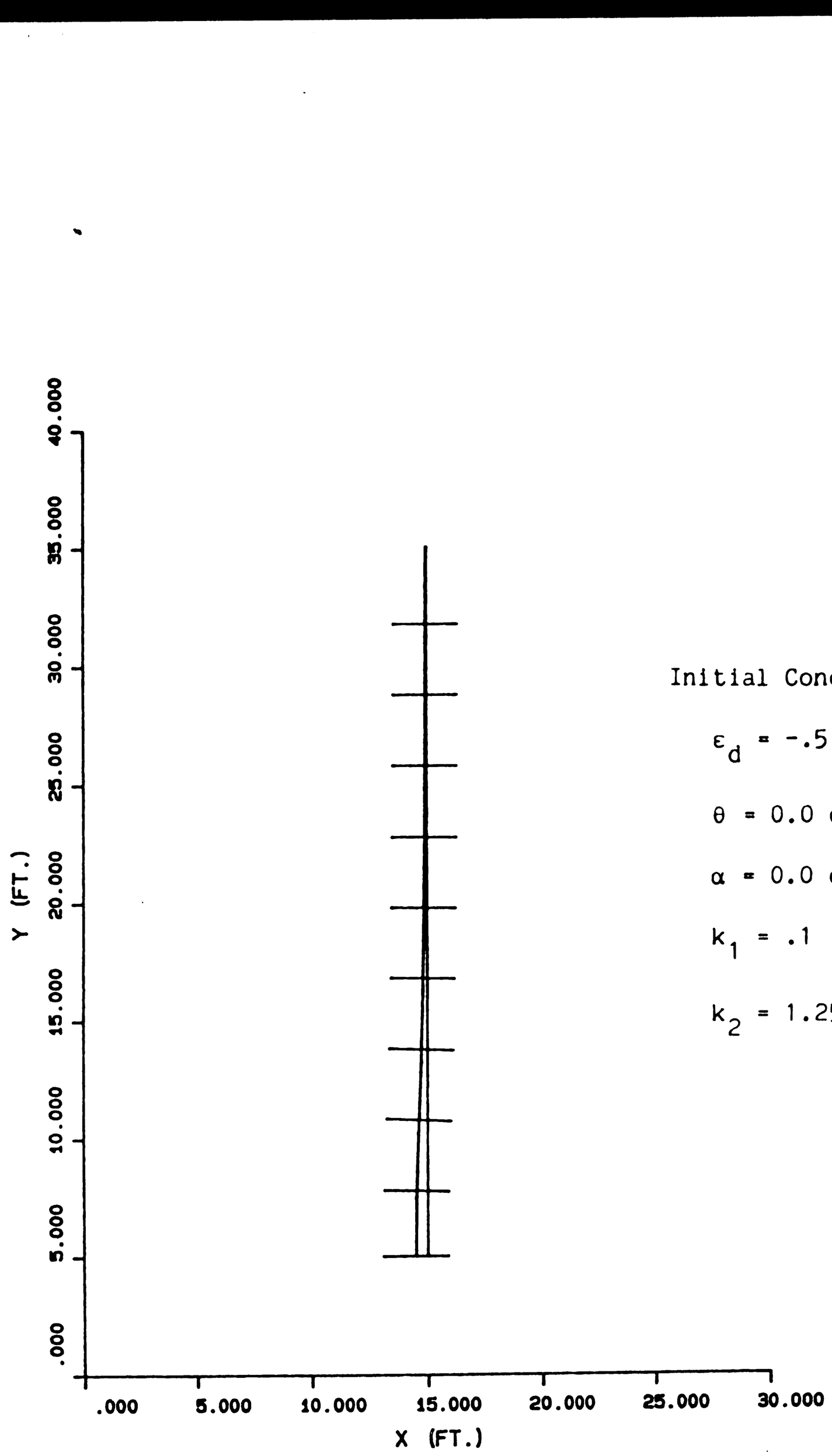

Figure 6: Straight line simulation (2)

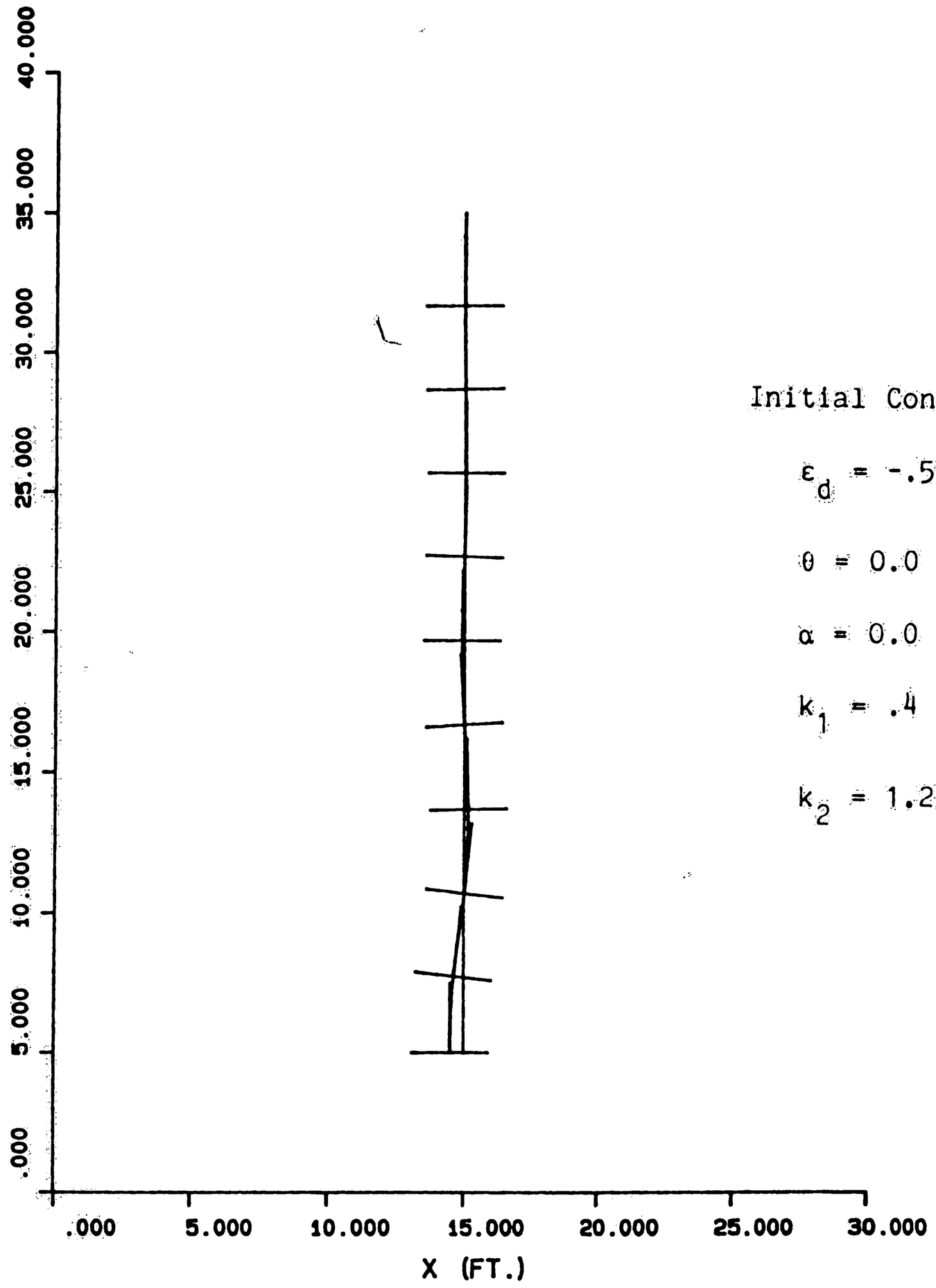

STRAIGHT LINE CONTROL

Figure 7: Straight line simulation (3)

Figure 8: Initial orientation error of 20.0 degrees. A slight orientation error can be seen at the end of the segment. The error comes as a result of the straight line controller assuming a constant point p velocity. The θ, x, and y equations take into account the change in $\dot{u}_p$ with the change in α, but $\dot{u}_p$ can never change in the straight line controller. The straight line controller moves to a straight line segment with a slightly different θ_k value than the actual physical segment. The offset error increases as the values of α increase, since $\dot{u}_p$ depends on the cosine of α. A check of the ε_d value output according to the straight line controller shows the value going to zero as time goes to infinity.

The graphical straight line simulation output can be used to determine how often the vehicle's absolute position must be updated.

Figure 9: Initial steering wheel angle of +15.0 degrees. The vehicle moves smoothly back to the straight line segment within 15.0 ft. of y-direction travel, and experiences no tracking error. No offset error is present because the straight line controller does not require large values of α to return to the straight line segment.

Figure 10: Initial position error of -.5 ft. initial orientation error of 20.0 degrees, and initial steering wheel angle of 15.0 degrees. Substantial tracking error is present because

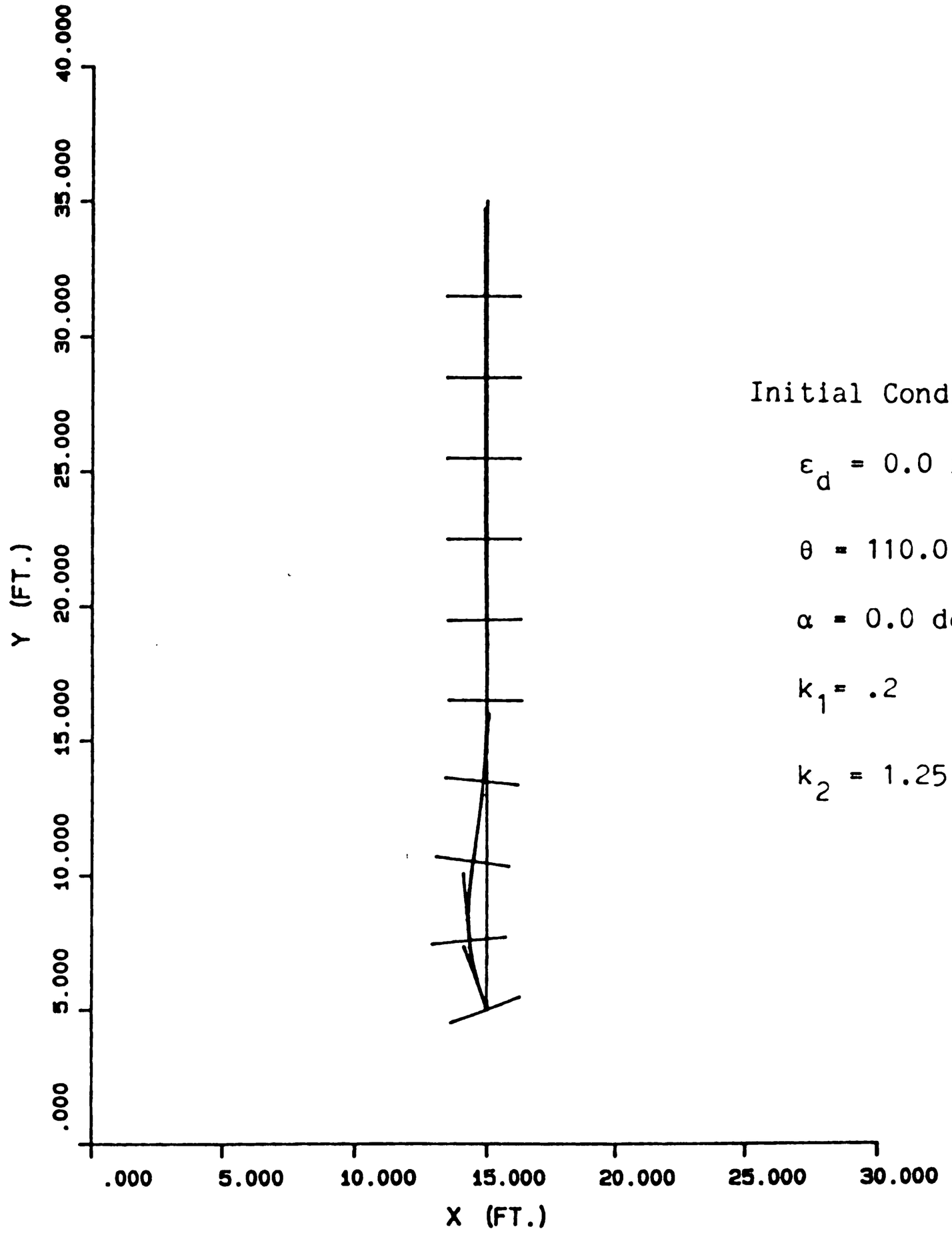

Figure 8: Straight line simulation (4)

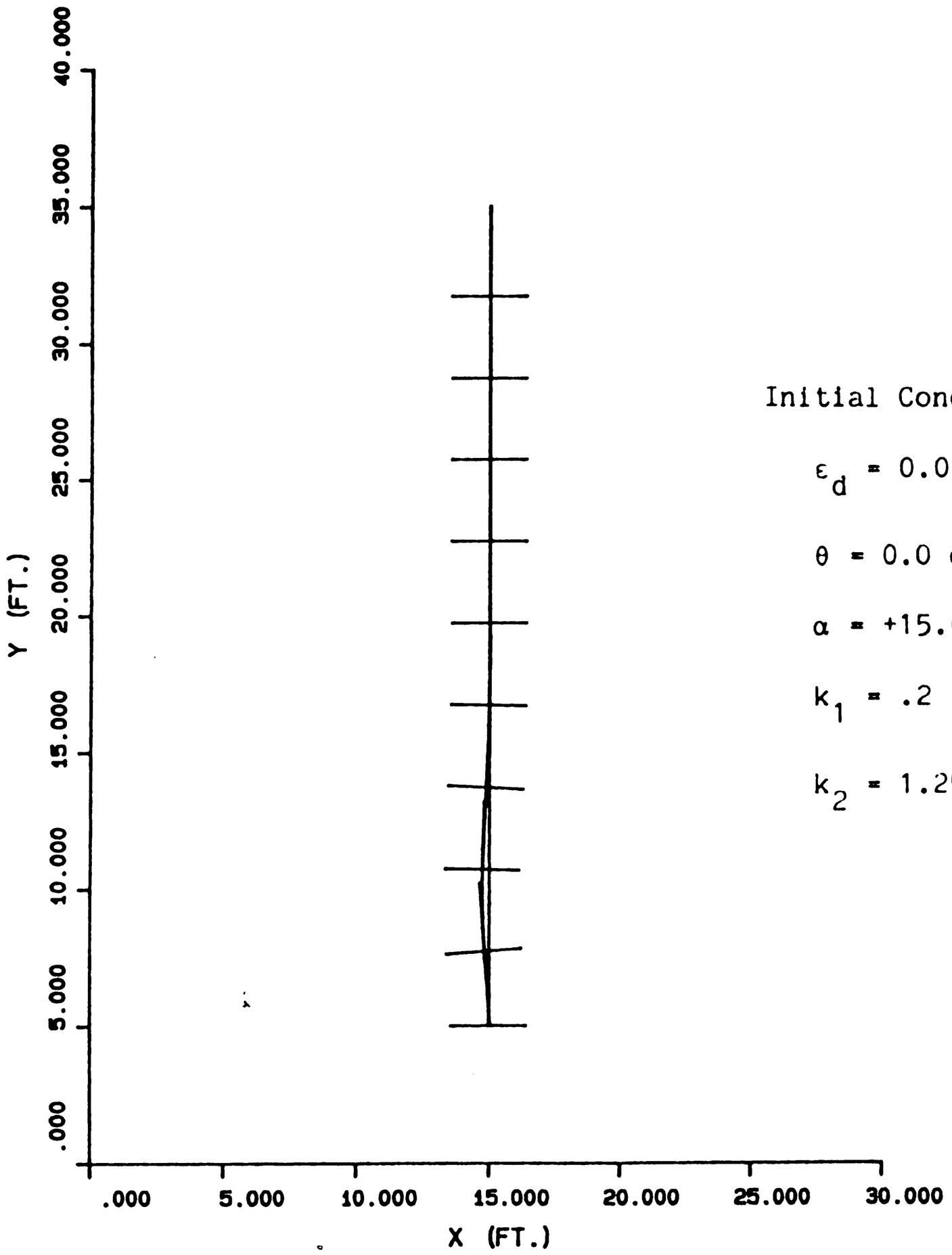

STRAIGHT LINE CONTROL

Figure 9: Straight line simulation (5)

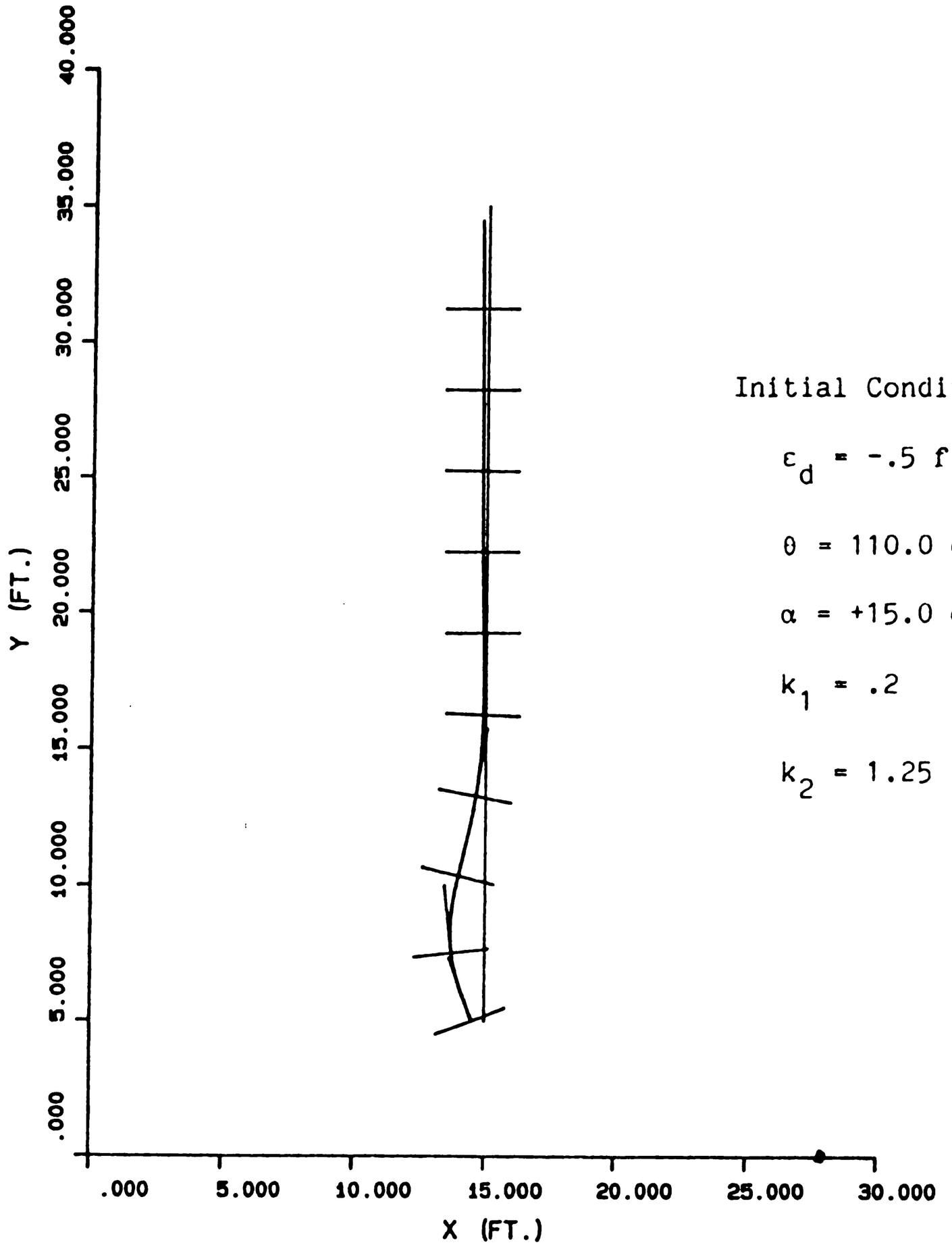

Initial Conditions:

ε_d = -.5 ft.

θ = 110.0 deg.

α = +15.0 deg.

k_1 = .2

k_2 = 1.25

STRAIGHT LINE CONTROL

Figure 10: Straight line simulation (6)

large values of α are required to right the vehicle from the initial configuration.

TURN SIMULATION:

Figure 11: The vehicle attempts a ninety degree turn and experiences overshoot and orientation error. The circled dot in Figures 11, 12, and 13 shows the position of the vehicle's point p at the end of the theoretical amount of turning time.

Figure 12: The τ_D parameter is set with k=.09. The vehicle's overshoot is eliminated while orientation error remains. The value of CON is zero.

Figure 13: The CON parameter is set at 2.54 and τ_D is equal to zero. The orientation error is essentially eliminated while the overshoot still exists.

Figure 14: The τ_D value is set with k=.09 and CON is set at 2.54. The turn overshoot and orientation error is eliminated.

COMPLETE SIMULATION:

The straight line controller gains are set at K_1=.2 and K_2=1.25.

Figure 15: Transition between two parallel straight line segments. The vehicle begins at the point 5,15.

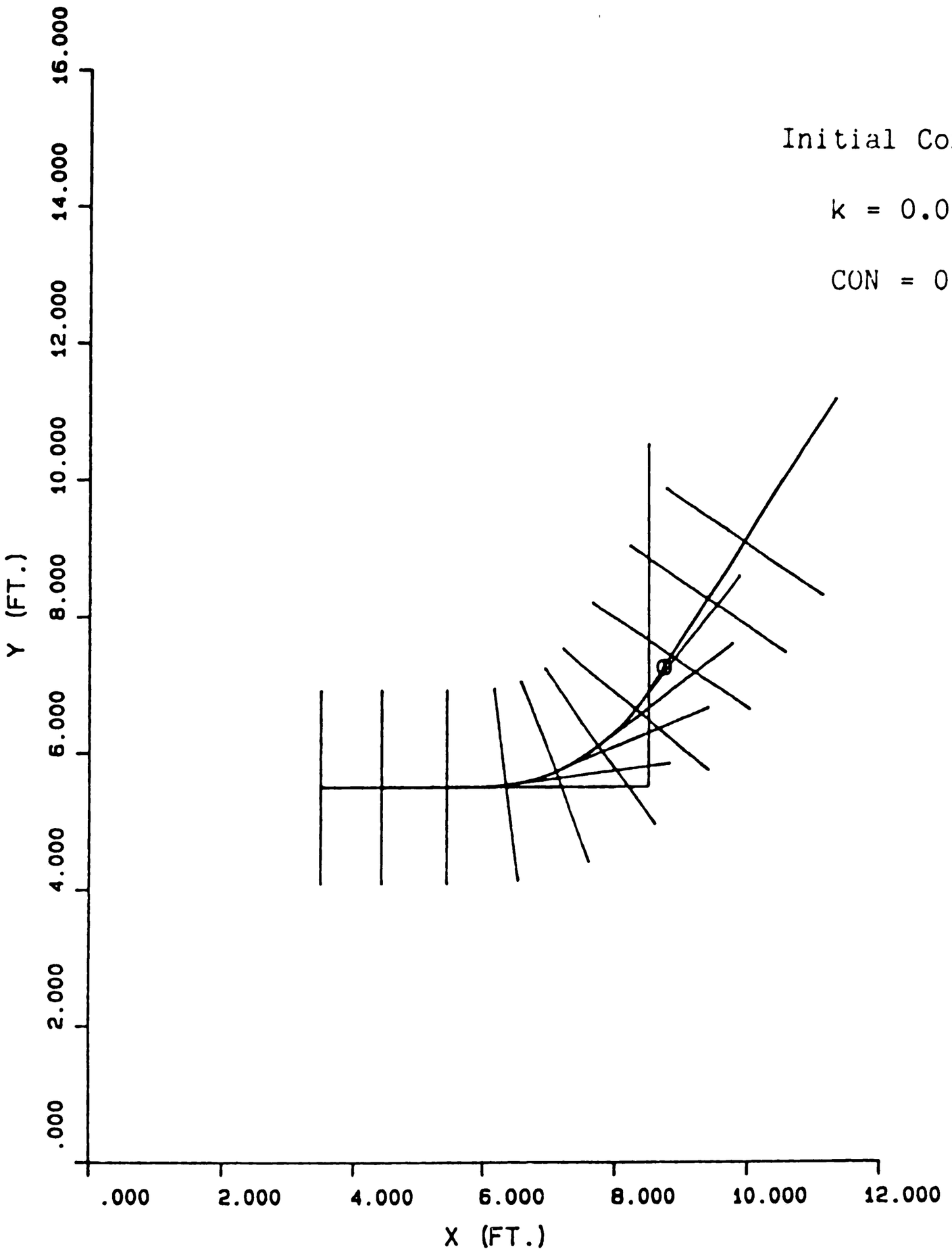

Figure 11: Turn simulation (1)

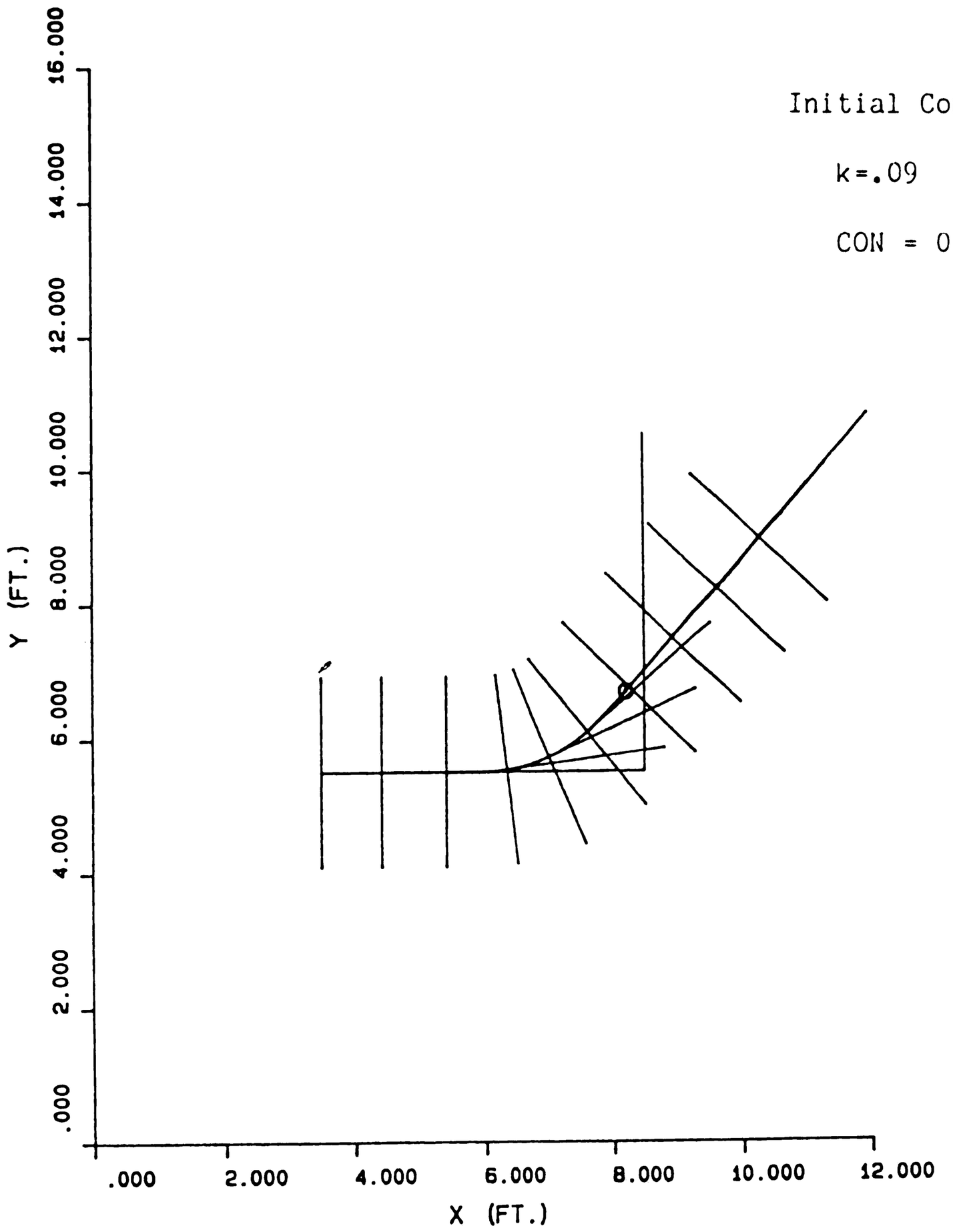

Figure 12: Turn Simulation (2)

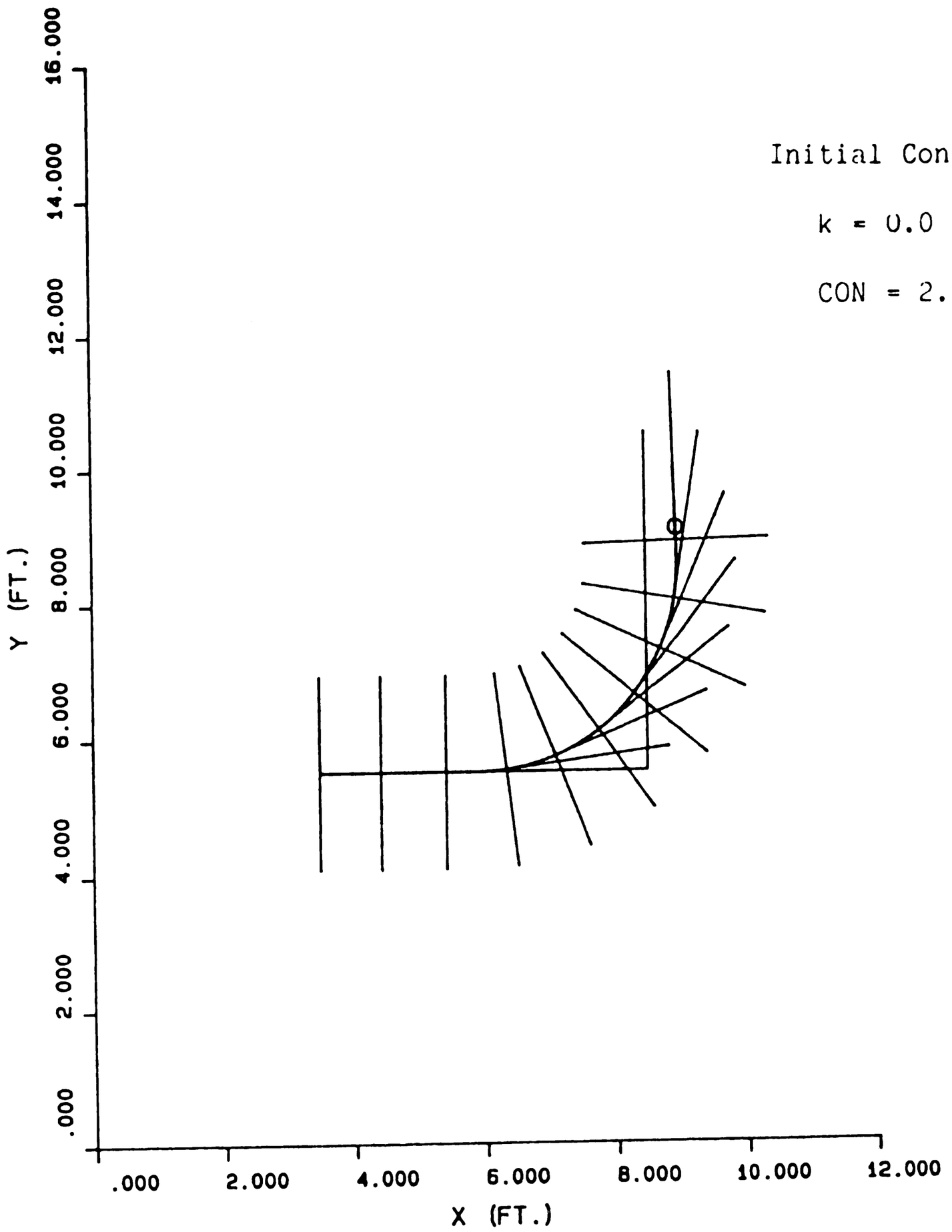

Figure 13: Turn simulation (3)

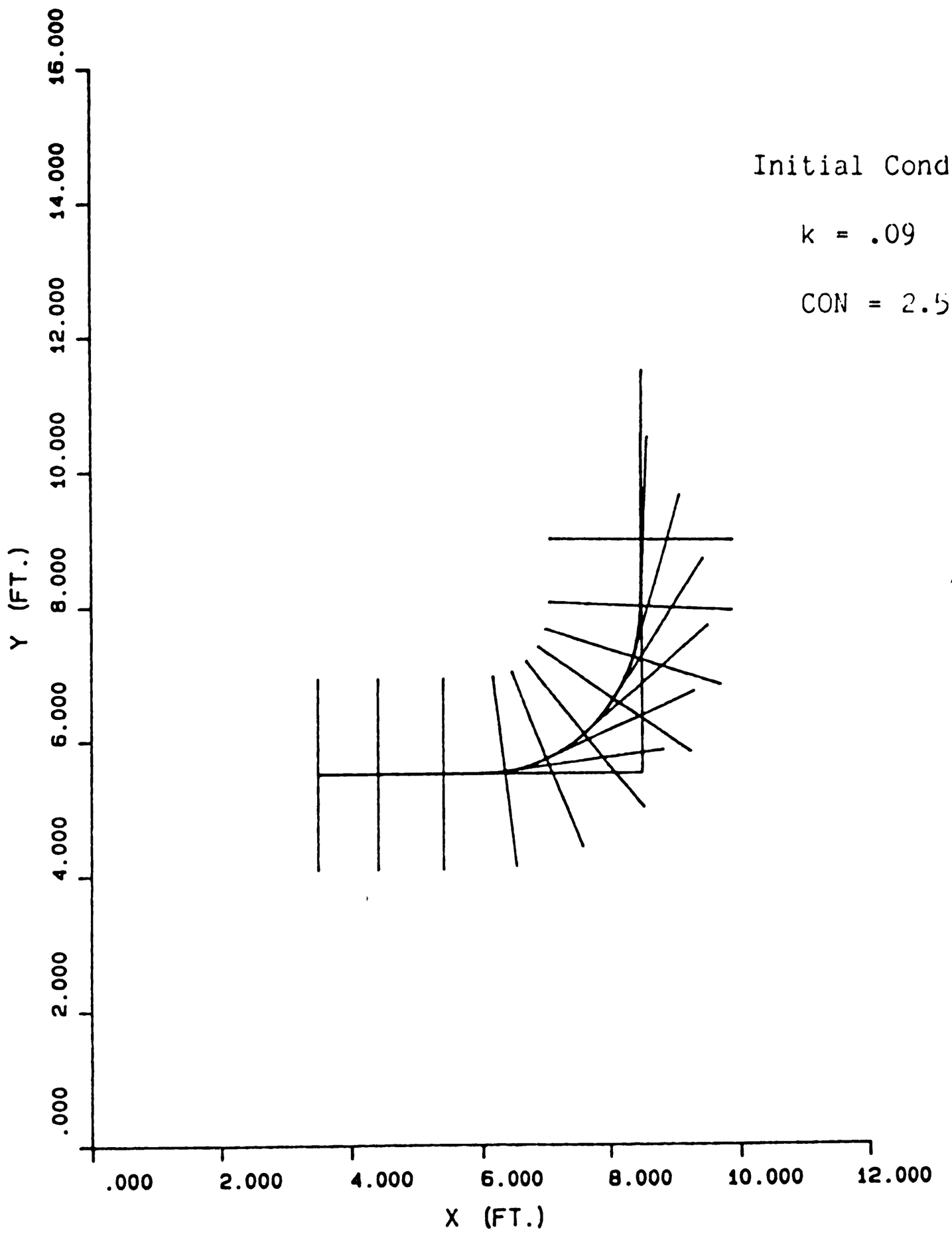

Figure 14: Turn simulation (4)

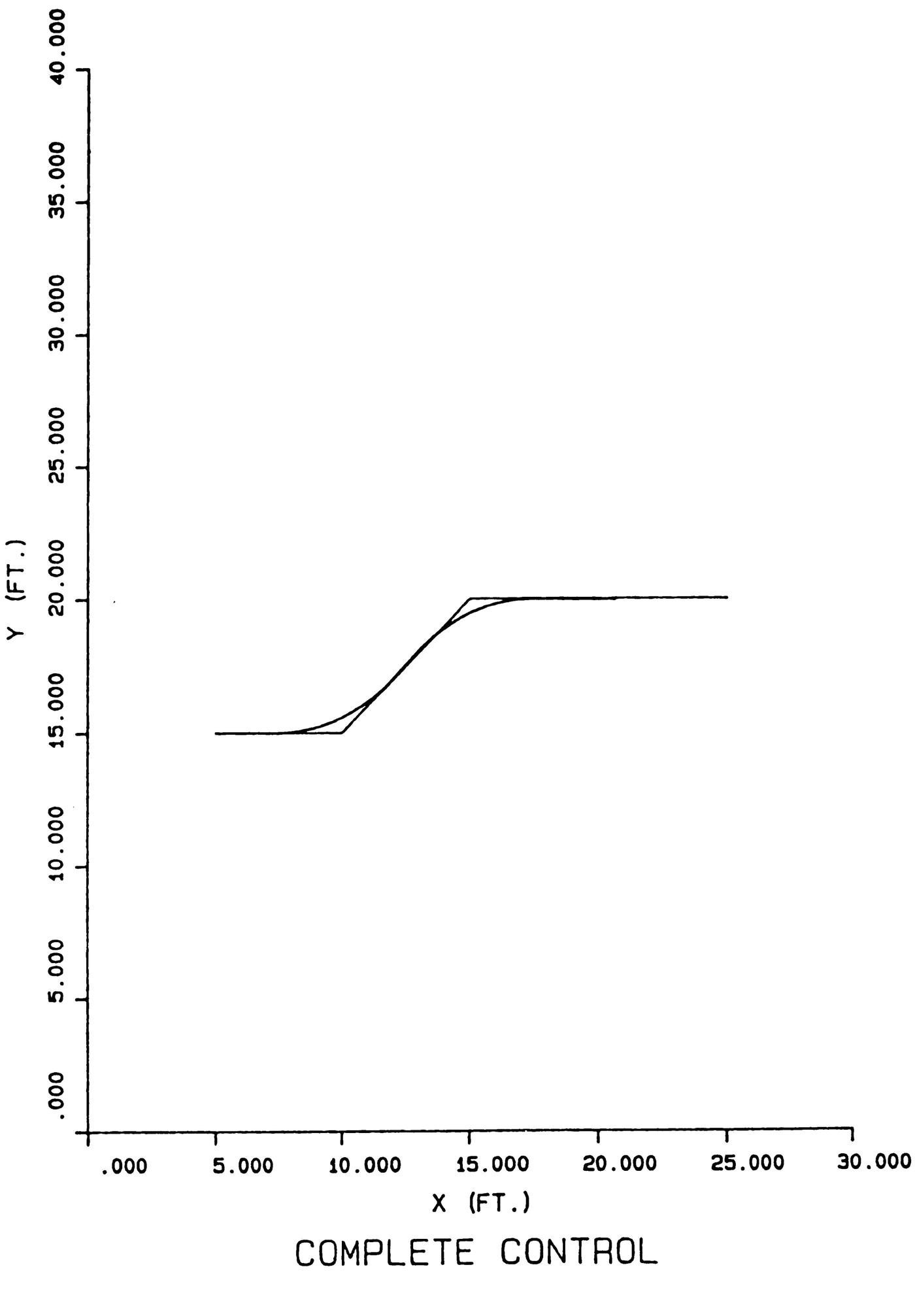

Figure 15: Complete simulation (1); Parallel segment transition

Figure 16: Completion of a bulb turn. The vehicle begins at the point 10,5.

Figure 17: Completion of a more typical plant floor trajectory. The vehicle begins at the point 5,5. Note the straight line controller offset error on the straight line segment at y equals 35 ft. The error is eventually righted since the x , y, and θ position variables are absolute (include the error).

Figure 16: Complete simulation (2); Bulb turn

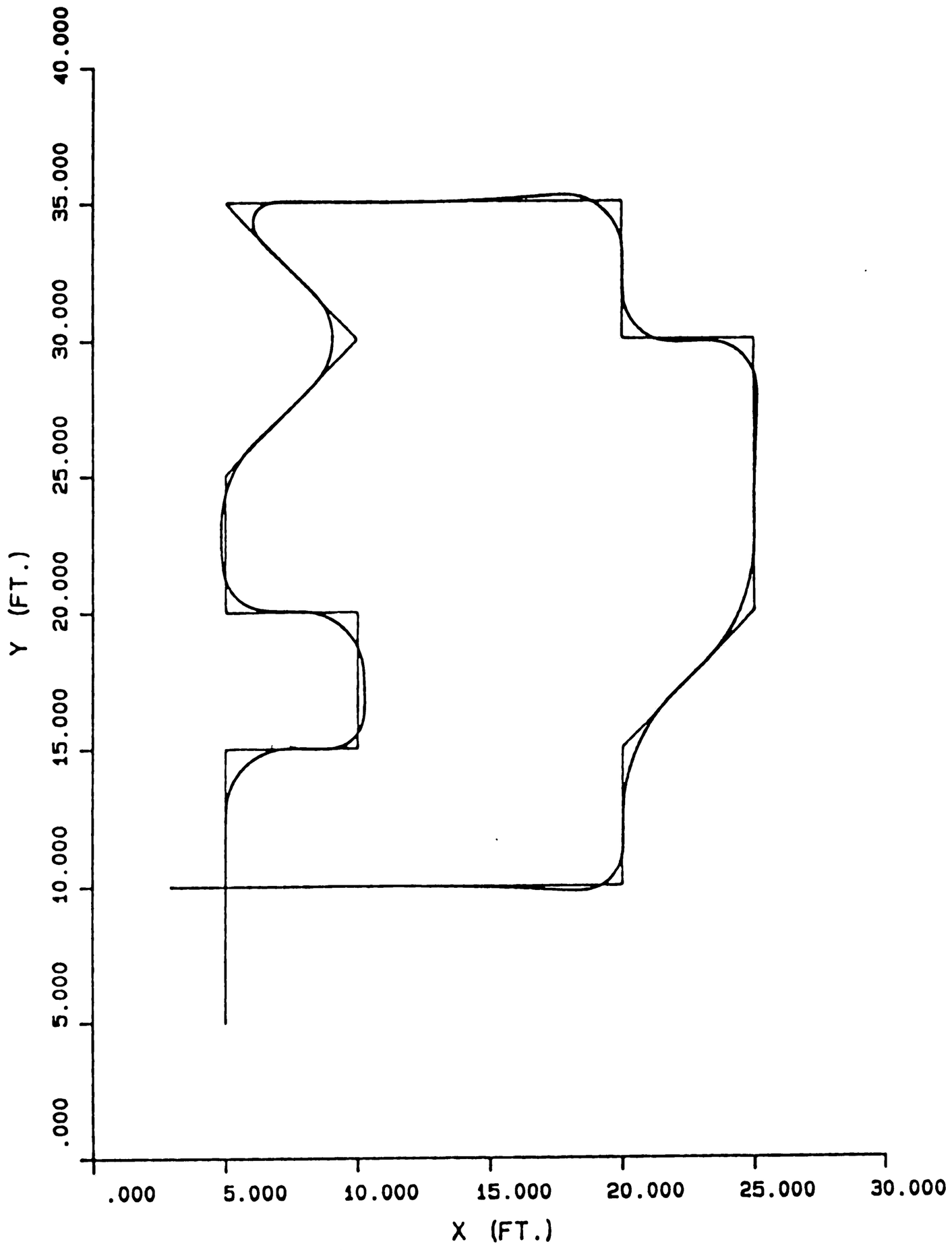

Figure 17: Compete simulation (3); Typical factory trajectory

RECOMMENDATIONS

The following are recommendations for future work.

1. A more detailed second order model of the steering assembly which includes damping. Frequency response methods can be used to model the assembly.

2. Determine the accuracy of the present kinematic model of the vehicle. The present simulation yields accumulated position errors without considering the vehicle's rolling dynamics. The current algorithms accuracy can be studied by mounting the Encoder Products Companies 7252 Motion Controller and shaft encoders on the present vehicle.

3. Continue development of complete control algorithm to include the vehicle's rolling dynamics. Include the slip angle investigation and decide if the slip effects are significant. Study improved algorithm with the vehicle and the motion controller. Consider the dead reckoning errors measured with and without the vehicle's rolling dynamics.

4. Develop advanced three dimensional dynamics equations which include actual center of gravity location, wheel loading shifts, and various floor materials.

5. Consider a velocity control algorithm and modify the straight line controller to include changing velocity.

6. Modify the complete control algorithm to switch from turn to straight line control after the vehicle reaches minimum ε_d and ε_θ values. The present algorithm switches according to the elapsed amount of time in the turn.

APPENDIX A: VEHICLE MODEL

The geometric model of the vehicle is pictured in Figure A-1.

The vehicle parameters are defined:

E: the distance between the centers of the rear wheels

L: the wheel base

R_r: radius of the rear wheels

R_f: radius of the front wheel

P: point defined by the intersection of the rear axle and the center line of the tricycle

Q: point about which the steering wheel pivots

θ: angular orientation of the vehicle measured between the fixed x-axis and the vehicle center line. Theta is measured positive in the counterclockwise direction with:

$$0 < \theta < 2\pi \ .$$

α: steering wheel angle. The angle is positive when the wheel turns to the left, and negative when the wheel turns to the right (viewed from the point p).

$\dot{u}_p$: velocity of the point p.

$\dot{u}_Q$: velocity of the point Q.

When the vehicle turns, it rotates about the point 0 and moves with a radius ρ. The radius is given by:

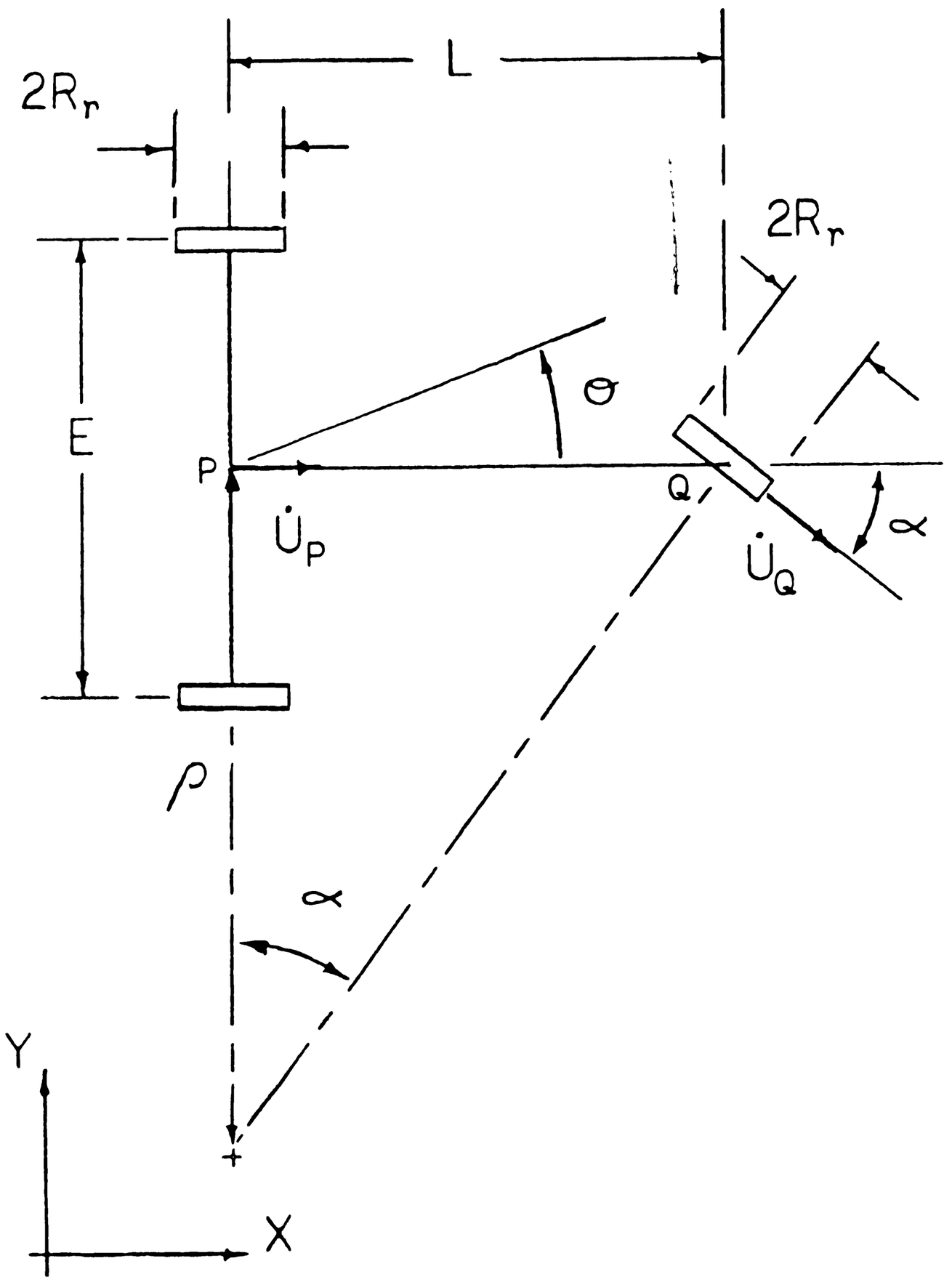

Figure A-1: Geometric model of vehicle

$$\rho = \frac{L}{\tan(\alpha)} \quad . \qquad (A\text{-}1)$$

APPENDIX B: SEGMENT IDENTIFICATION AND POSITION EQUATIONS

SEGMENT IDENTIFICATION:

All segments are identified by a beginning and an ending x and y coordinate value, an angular orientation θ_k, and a length L_k relative to the fixed reference frame. The segment orientation is defined positive in the counterclockwise direction and:

$$0 < \theta_k < 2\pi \ .$$

The segment orientation is given by:

$$\theta_k = \tan^{-1}\left[\frac{PY(k+1)-PY(k)}{PX(k+1)-PX(k)}\right] . \qquad (B\text{-}1)$$

The segment length is found using:

$$L_k^2 = (PY(k+1)-PY(k))^2 + (PX(k+1)-PX(k))^2 . \qquad (B\text{-}2)$$

A series of n segments are numbered from 1 to n. The segment identification convention is shown in Figure B-1.

POSITION AND ORIENTATION ERRORS RELATIVE TO CURRENT PATH SEGMENT:

The vehicle's error from the current path segment is given by position error, ε_d, and orientation error, ε_θ. Position error ε_d is the perpendicular distance from the point p to the current path segment. The quantity ε_d is positive to the right of a segment, and negative to the left of a segment.

The orientation error is given by:

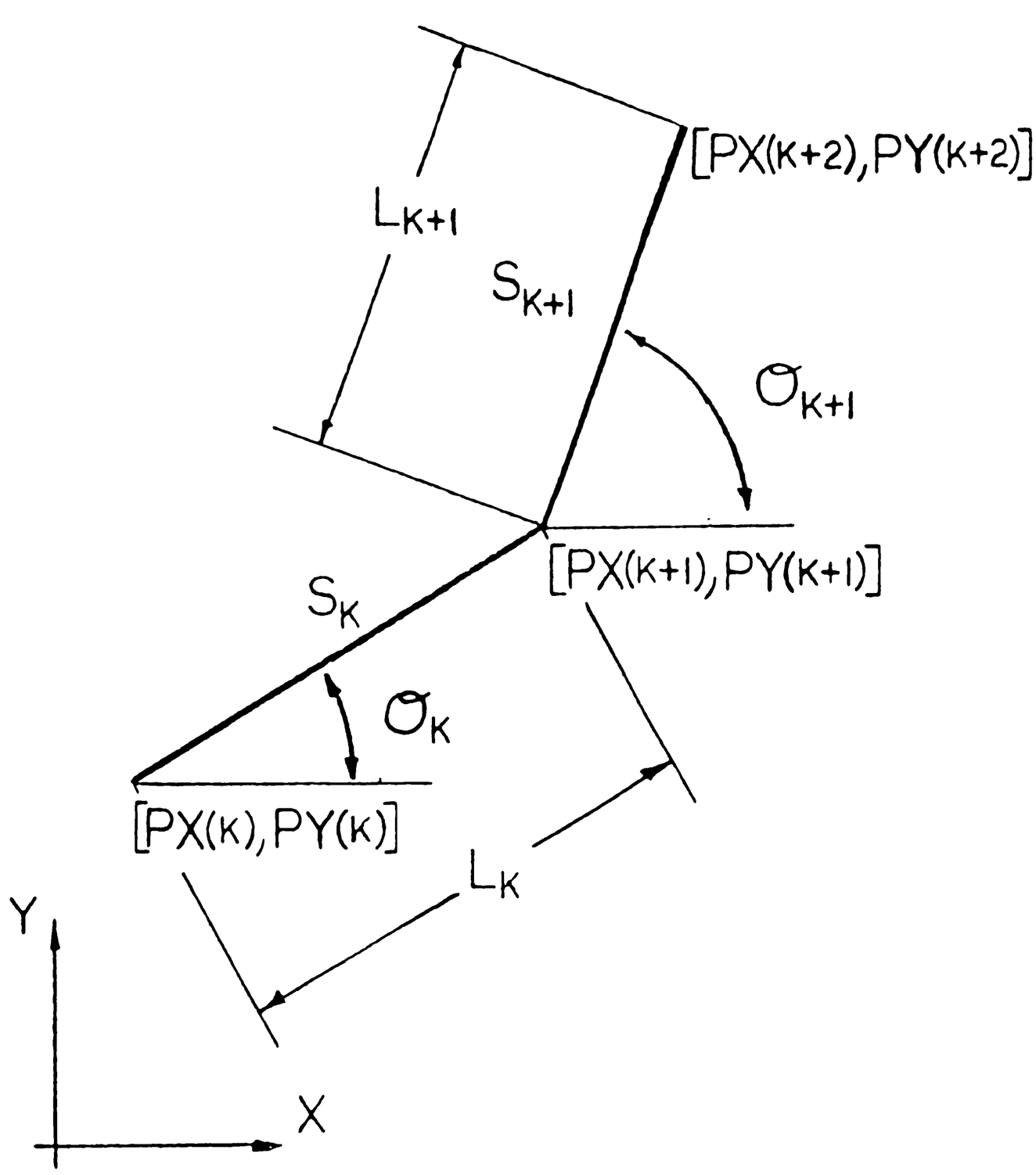

Figure B-1: Segment identification convention

$$\varepsilon_\theta = \theta_k - \theta \ . \qquad (B\text{-}3)$$

The position and orientation errors relative to the current path segment are pictured in Figure B-2.

STARRED COORDINATE SYSTEM:

Another coordinate system called the starred coordinate system is attached to each path segment. The starred coordinate systems allows calculation of the vehicle's x-y position relative to the next path segment. The orientation and position of the starred coordinate system is shown in Figure B-3.

POSITION AND ORIENTATION ERRORS RELATIVE TO THE NEXT PATH SEGMENT:

The position error relative to the next path segment, $\hat{\varepsilon}_d$, is given by:

$$\hat{\varepsilon}_d = x^* \cos(\theta_{k+1}-\theta_k) - (L_k - y^*)\sin(\theta_{k+1}-\theta_k) \ . \qquad (B\text{-}4)$$

The orientation error relative to the next path segment, $\hat{\varepsilon}_\theta$, is given by:

$$\hat{\varepsilon}_\theta = \theta_{k+1} - \theta \ . \qquad (B\text{-}5)$$

When the controllers switch from the k segment to the k+1 segment, the new position error is $\hat{\varepsilon}_d$, and the new orientation error is $\hat{\varepsilon}_\theta$.

The position errors relative to the next path segment are shown in Figure B-4.

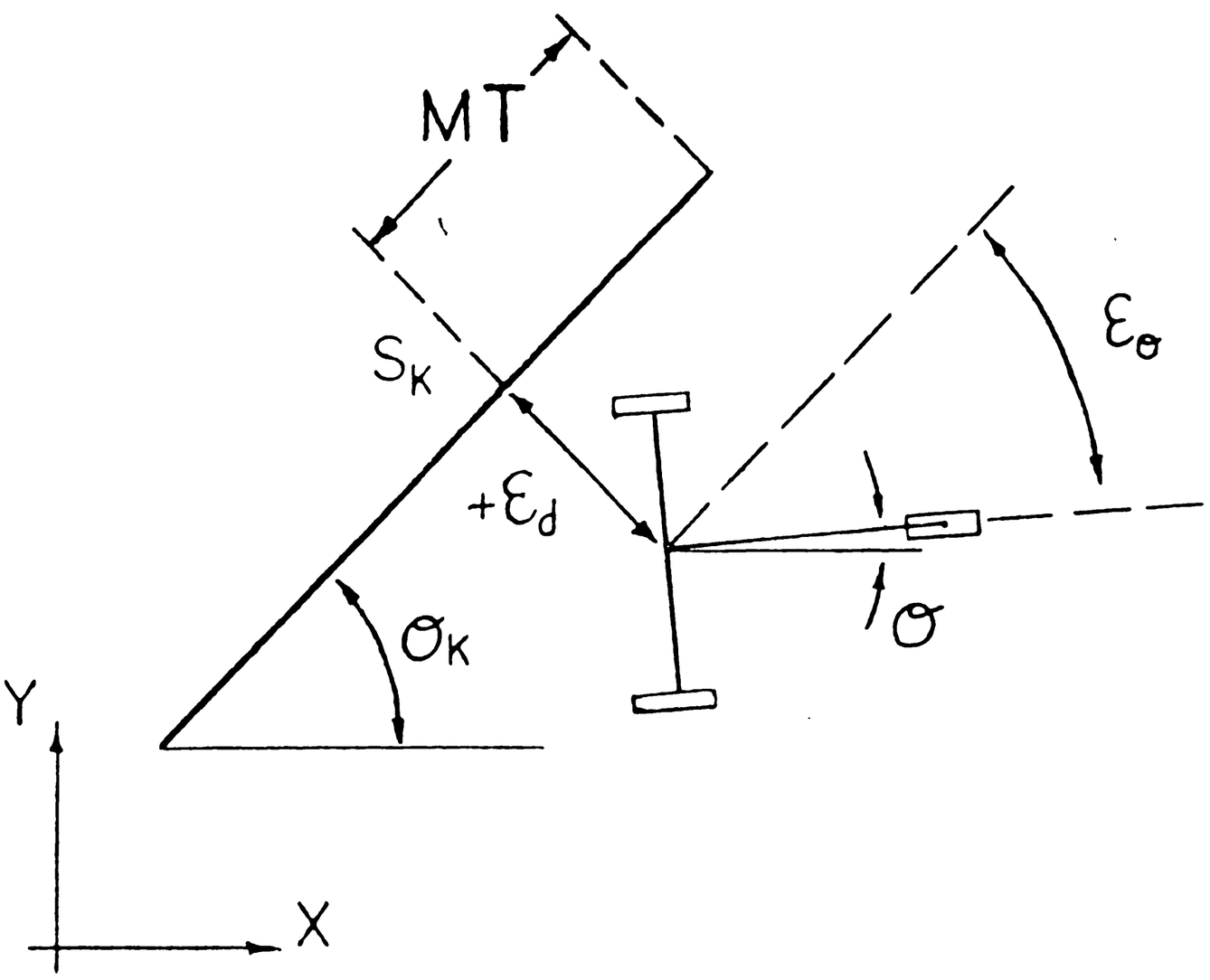

Figure B-2: Errors relative to current segment

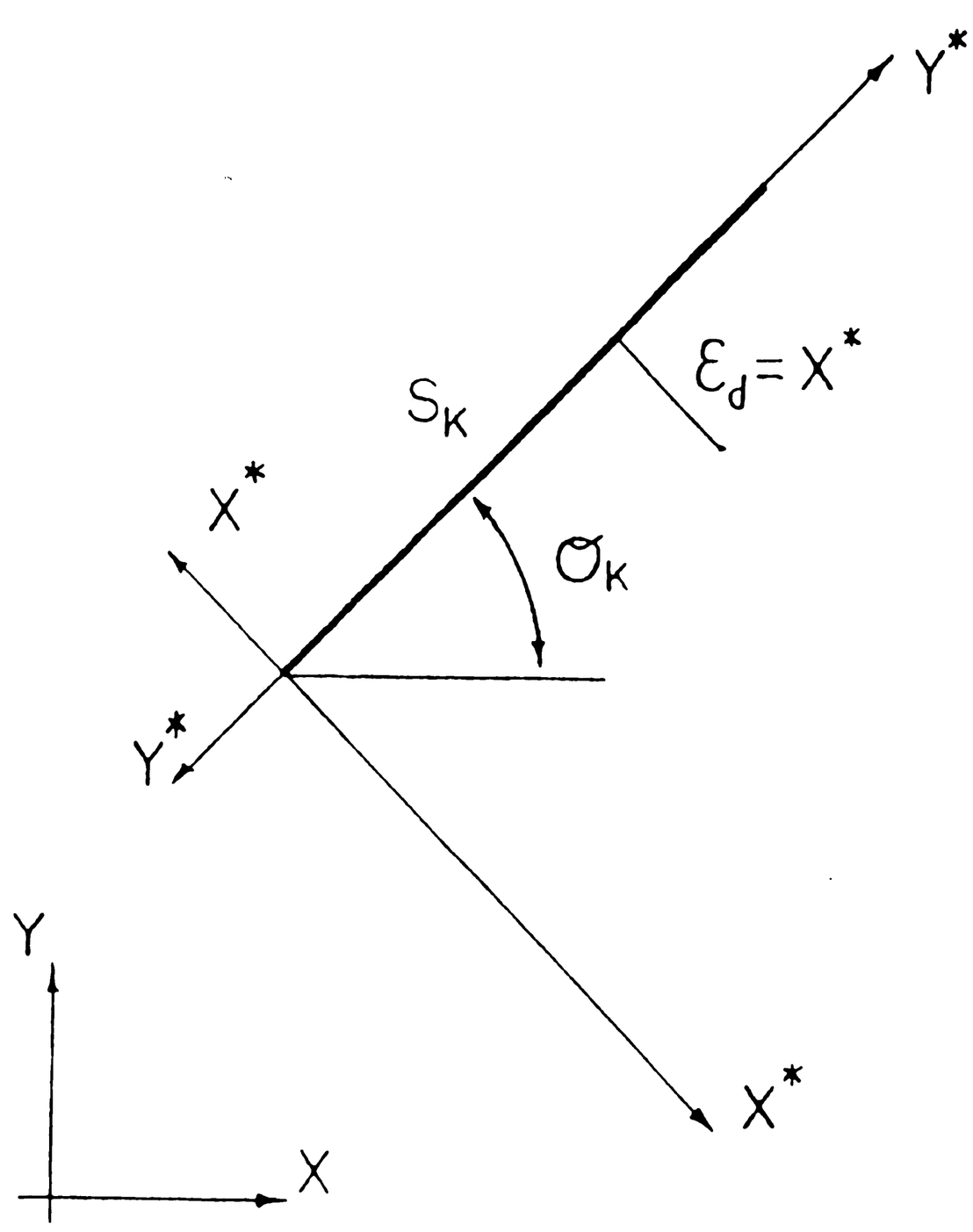

Figure B-3: Starred coordinate system

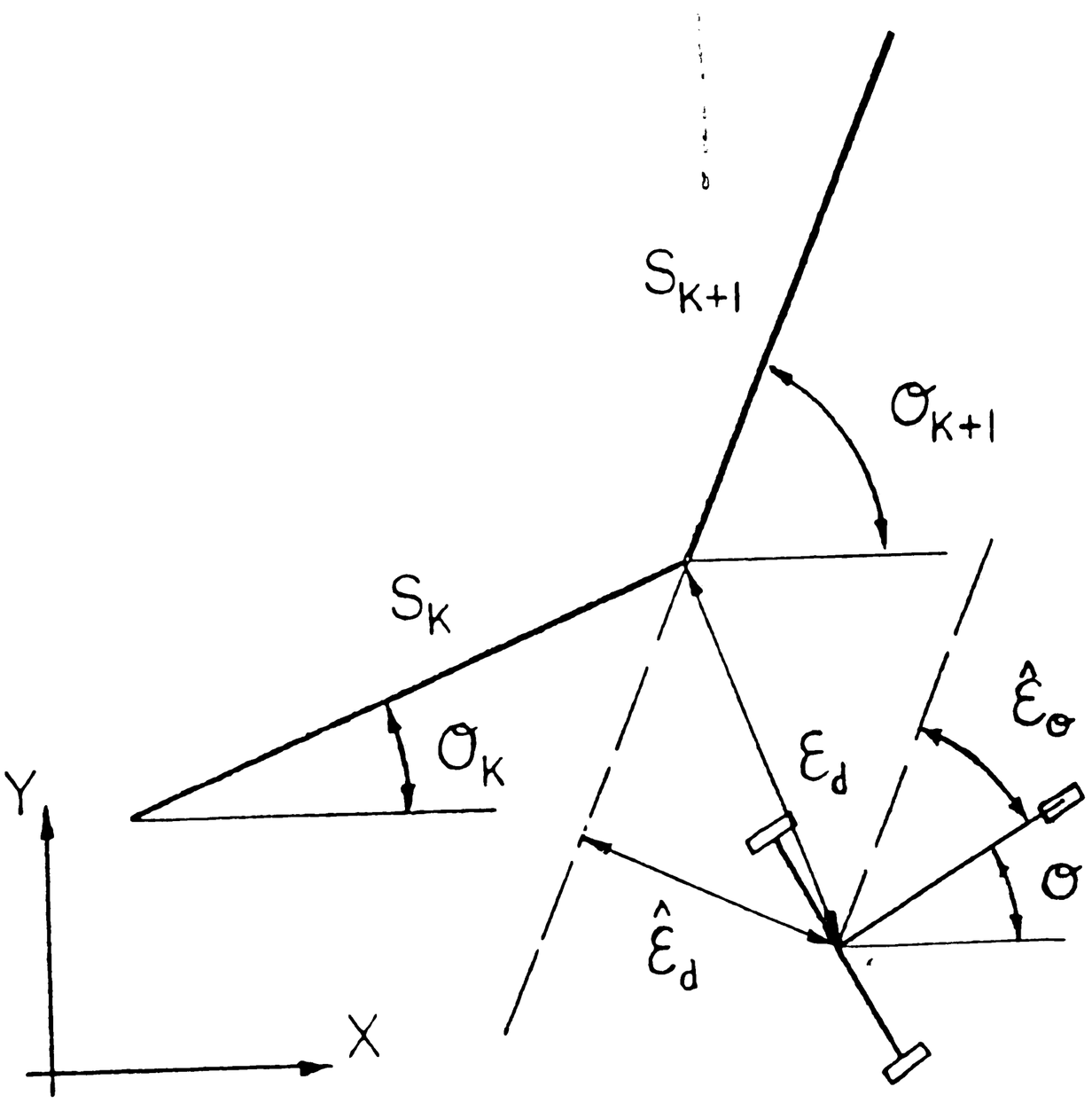

Figure B-4: Errors relative to the next segment

DETERMINATION OF x^* AND y^* GIVEN x, y, PX(k), PY(k) AND θ_k:

In calculating the vehicle's position error relative to the next path, x^* and y^* are needed. To calculate x^* and y^* the vehicle's x and y position must be known, as well as the current path segments initial x-y point and orientation. The starred coordinates are given by:

$$x^* = x\sin\theta_k - y\cos\theta_k - PX(k)\sin\theta_k + PY(k)\cos\theta_k \ , \qquad (B\text{-}6)$$

$$y^* = x\cos\theta_k + y\sin\theta_k - PX(k)\cos\theta_k - PY(k)\sin\theta_k \ . \qquad (B\text{-}7)$$

Equations B-6 and B-7 are developed using standard coordinate transformations.

APPENDIX C: DERIVATION OF GOVERNING STRAIGHT LINE EQUATIONS

The equations which govern the motion of the AGV during straight line travel are derived by describing the vehicle's position error ε_d, and the orientation error ε_θ. Small perturbations in ε_d and ε_θ are assumed.

Assuming small perturbations in ε_d and ε_θ allows the steering angle, α, to also be assumed small. With α small:

$$\tan\alpha \approx \alpha \ , \qquad (C\text{-}1)$$

and

$$\cos\alpha \approx 1 \ . \qquad (C\text{-}2)$$

Also since ε_θ is assumed to be approximately equal to zero:

$$\sin\varepsilon_\theta \approx \varepsilon_\theta \ . \qquad (C\text{-}3)$$

Expressions for ε_d and ε_θ are determined in terms of the vehicle parameters and steering wheel angle α. Noting Figure B-2:

$$\dot{\varepsilon}_d = \dot{u}_p \sin\varepsilon_\theta \ , \qquad (C\text{-}4)$$

or since ε_θ is small,

$$\dot{\varepsilon}_d \approx \dot{u}_p \varepsilon_\theta \ . \qquad (C\text{-}5)$$

Since $\dot{u}_p$ is considered a constant for the straight line controller, the second derivitive of ε_d is written:

$$\ddot{\varepsilon}_d \approx \dot{u}_p \dot{\varepsilon}_\theta \ . \qquad (C\text{-}6)$$

Using the relationship between the vehicle's linear and angular velocity, the vehicle's turning radius is written:

$$\rho = \frac{\dot{u}_p}{\dot{\theta}} \quad . \qquad (C\text{-}7)$$

Using the expression for ρ developed in Appendix A, equation C-7 can be written:

$$\rho = \frac{\dot{u}_p}{\dot{\theta}} = \frac{L}{\tan\alpha} \quad . \qquad (C\text{-}8)$$

Since α is small:

$$\dot{\theta} = \frac{\dot{u}_p}{L}\,\alpha \quad . \qquad (C\text{-}9)$$

Next, θ can be related to ε_θ by taking the time derivative of ε_θ:

$$\dot{\varepsilon}_\theta = \frac{d}{dt}\,(\theta_k - \theta) = -\dot{\theta} \quad . \qquad (C\text{-}10)$$

Substituting equations C-10 into equation C-6:

$$\ddot{\varepsilon}_d = -\frac{\dot{u}_p^2}{L}\,\alpha \quad . \qquad (C\text{-}11)$$

Utilizing the Laplace Domain with equations C-10 and C-11, the transfer functions between $\varepsilon_d(s)$ and $\alpha(s)$ and $\varepsilon_\theta(s)$ and $\alpha(s)$ are written:

$$\frac{\varepsilon_{d(s)}}{\alpha(s)} = -\frac{\dot{u}_p^2}{Ls^2} = G_{1(s)} \quad , \qquad (C\text{-}12)$$

and

$$\frac{\varepsilon_{\theta(s)}}{\alpha(s)} = -\frac{\dot{u}_p}{Ls} = G_2(s) \ . \qquad (C\text{-}13)$$

The third order differential equation which governs the motion of the vehicle during straight line motion is now developed using equation C-14:

$$\frac{\alpha_{(s)}}{C_{\alpha(s)}} = \frac{1}{1+\tau s} \ , \qquad (C\text{-}14)$$

and equation C-15:

$$C_\alpha(s) = k_1(\varepsilon_d(s)^{set} - \varepsilon_d(s)) + k_2(\varepsilon_\theta(s)^{set} - \varepsilon_\theta(s)) \ . \qquad (C\text{-}15)$$

Recall that the set point values are equal to zero. Moving back to the time domain and substituting equation C-15 into equation C-14 produces:

$$C_\alpha(t) = \alpha(t) + \tau \frac{d_{\alpha(t)}}{dt} = +k_1\varepsilon_d(t) + k_2\varepsilon_\theta(t) \ . \qquad (C\text{-}16)$$

Using equation C-11, expressions for $\alpha(t)$ and $\frac{d_{\alpha(t)}}{dt}$ are written:

$$\alpha(t) = -\frac{L}{\dot{u}_p^2} \ddot{\varepsilon}_{d(t)} \ , \qquad (C\text{-}17)$$

and

$$\frac{d_{\alpha(t)}}{dt} = -\frac{L}{\dot{u}_p^2} \dddot{\varepsilon}_{d(t)} \ . \qquad (C\text{-}18)$$

Substituting equations C-6, C-17, and C-18 into C-16 produces a third order differential equation in ε_d:

$$\dddot{\varepsilon}_{d(t)} + \frac{1}{\tau}\ddot{\varepsilon}_{d(t)} + \frac{k_2\dot{u}_p}{\tau L}\dot{\varepsilon}_{d(t)} + \frac{k_1\dot{u}_p^2}{\tau L}\varepsilon_{d(t)} = 0 \text{ [4]}. \quad (C\text{-}19)$$

Note the initialization of D1, D2, and D3 in equation C-21 are used to initialize the position of the vehicle at time equal to zero in the simulation. Initial position error is set through D1, initial orientation error is set through D2 and equation C-5, and initial steering wheel angle is set through D3 using equation C-11. Care must be taken in initializing the sign of D2 so that the vehicle's initial velocity is correct relative to the current path segment.

The third order equation is simulated using a system of three first order equations. The variable substitutions made are:

$$\varepsilon_{d(t)} = D1$$

$$\dot{\varepsilon}_{d(t)} = D2 = \dot{D1}$$

$$\ddot{\varepsilon}_{d(t)} = D3 = \dot{D2} \quad (C\text{-}20)$$

$$\dddot{\varepsilon}_{d(t)} = D4 = \dot{D3} .$$

The three first order equations are:

$$\dot{D1} = D2$$

$$\dot{D2} = D3 \quad (C\text{-}21)$$

$$\dot{D3} = -\frac{1}{\tau} D3 - \frac{k_2\dot{u}_p}{\tau L} D2 - \frac{k_1\dot{u}_p^2}{\tau L} D1 .$$

ROOT CONTOUR GAIN CALCULATION:

The root contour analysis is used to theoretically determine the values of the gains k_1 and k_2. The root contour analysis differs from the traditional root locus analysis in that more than one gain value is varied. The analysis presented here, determines the gain values for the system to be critically damped.

The actual gain values were determined through simulation. The simulation produced the vehicle's straight line trajectory according to equation C-21. The k_1 and k_2 gains were varied until a desired trajectory was produced. Note, the theoretical gain values were used as starting values in the simulation.

Block diagram reduction of Figure 1 produces the relationship between $\varepsilon_{d(s)}$, $\varepsilon_d^{set}(s)$ and $\varepsilon_\theta^{set}(s)$:

$$\varepsilon_{d(s)} = \frac{G_{v(s)}G_{1(s)}k_1}{1+G_{v(s)}(k_1G_{1(s)}+k_2G_{2(s)})}\varepsilon_d^{set}(s) + \frac{G_{v(s)}G_{1(s)}k_2}{1+G_{v(s)}(k_1G_{1(s)}+k_2G_{2(s)})}\varepsilon_\theta^{set}(s) . \qquad (C\text{-}22)$$

If $\varepsilon_d^{set}(s)$ and $\varepsilon_\theta^{set}(s)$ are set equal to zero and the time domain is utilized, equation C-22 becomes equation C-19.

The third order closed loop characteristic equation of the system is:

$$1 + G_{v(s)}(k_1 G_{1(s)} + k_2 G_{2(s)}) \quad . \qquad (C\text{-}23)$$

Substituting $G_{v(s)}$, $G_{1(s)}$, and $G_{2(s)}$, equation C-23 becomes:

$$1 + \frac{\frac{k_2 \dot{u}_p}{L\tau}\left(s + \frac{k_1 \dot{u}_p}{k_2}\right)}{s^2\left(s + \frac{1}{\tau}\right)} = 0 \quad . \qquad (C\text{-}24)$$

The root locus of equation 24 appears in Figure C-1. Note the locus is drawn with the zero positioned inside of the left most pole. The exact shape of the locus is determined by the values of k_1 and k_2.

The root contour analysis attempts to approximate the third order system as a second order system and determine the values of k_1 and k_2 such that the system is critically damped (ξ=1.0). The steps in the root locus analysis are:

(1). Set k_1=0 in the closed loop characteristic equation and vary k_2. Draw the corresponding root locus.

(2). With k_2 set from step (1), let k_1 vary in the closed loop characteristic equation. Draw the corresponding locus. Note, the open loop poles of the second locus are the closed loop roots of the first locus.

(3). Position the poles of the second locus to produce critical damping. Determine the values of k_1 and k_2.

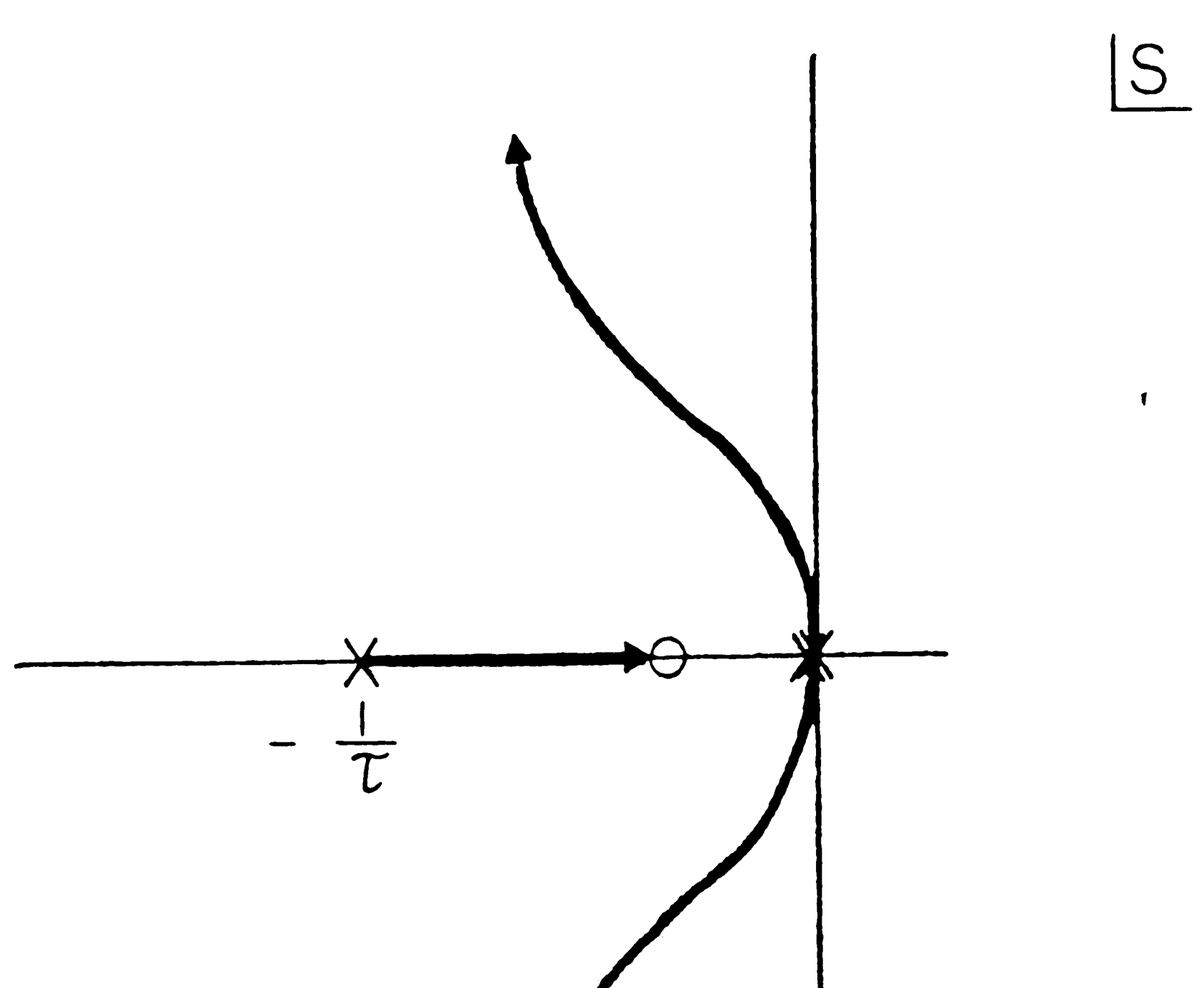

Figure C-1: Root locus of characteristic equation

Step (1) changes equation C-24 to:

$$1 + \frac{\frac{k_2 \dot{u}_p}{\tau L}}{s(s+1/\tau)} = 0 \ , \qquad (C\text{-}25)$$

with the locus drawn in Figure C-2. Step (2) changes equation C-24 to:

$$1 + \frac{\frac{k_1 \dot{u}_p^{\,2}}{\tau L}}{s(s^2 + \frac{1}{\tau} s + \frac{k_2 \dot{u}_p}{\tau L})} = 0 \ , \qquad (C\text{-}26)$$

with the locus drawn in Figure C-3. Note the start of the locus in Figure C-3 is determined by k_2, or the quantity in parenthesis in equation C-26.

The poles of the first locus are trapped at the breakaway point, or at:

$$s = -\frac{1}{2\tau} \ . \qquad (C\text{-}27)$$

With the s value in equation C-27, k_2 is determined to be:

$$k_2 = \frac{L}{4\tau \dot{u}_p} \ . \qquad (C\text{-}28)$$

The second locus now begins at the breakaway point and is a real number with no imaginary parts. The k_1 value is determined from equation C-26 once the value of s is known at the breakaway point. The value of s is determined by the fact that:

$$\frac{dk_1}{ds} = 0 \ , \qquad (C\text{-}29)$$

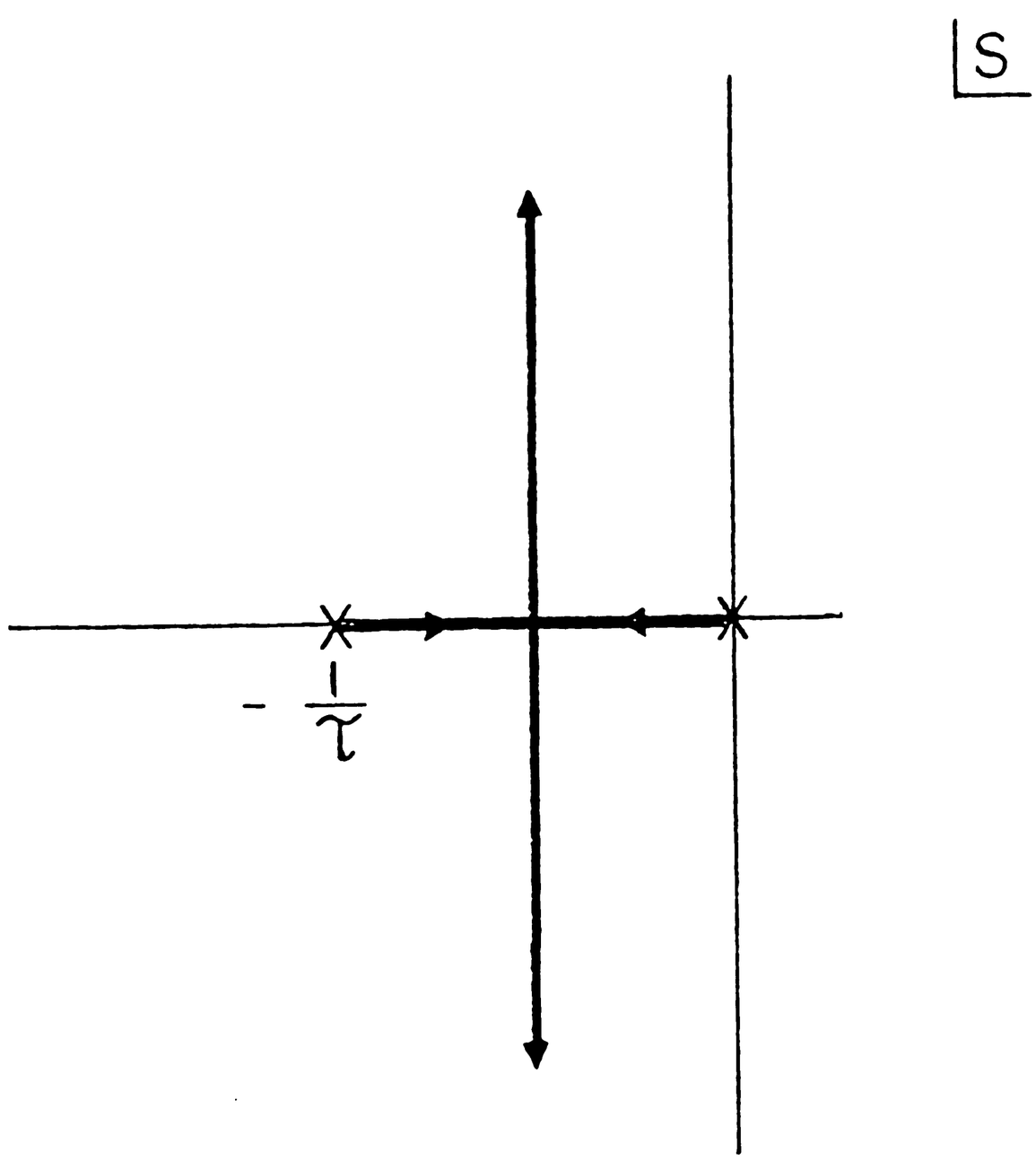

Figure C-2: Root locus with k_1 equal to zero

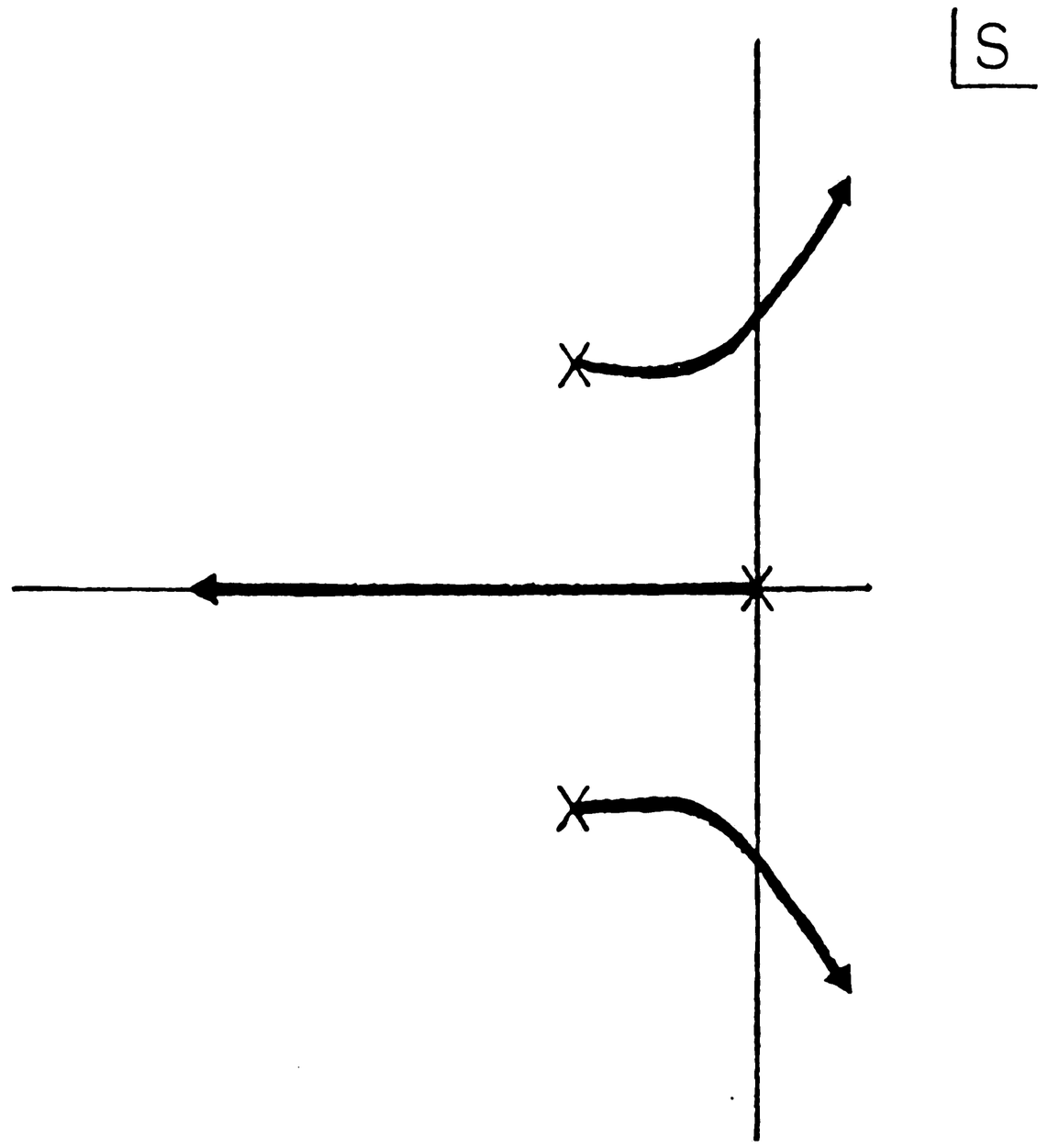

Figure C-3: Root locus with k_1 varying

at the breakaway.

Using the quadratic equation, the value of s at the breakaway is:

$$s = -\frac{1}{6\tau} . \qquad (C-30)$$

Substituting equation C-30 into equation C-26 produces:

$$k_1 = \frac{.0185L}{\dot{u}_p^2 \tau^2} . \qquad (C-31)$$

The expressions for k_1 and k_2 produces a critically damped system.

Consider the effects of varying the k_1 and k_2 gain values. As k_2 is increased past the k_2 value found at the breakaway point, the second locus begins with a greater complex root value. The effect of increasing k_2 is less damping, more overshoot, and decreased rise-time. As k_1 is increased the roots on the second locus move more and more toward the right half plane and eventually cross the imaginary axis. Too large a value of k_1 will cause unstable response, and the vehicle will oscillate away from a given straight line segment.

APPENDIX D: TURNING CONTROL

DERIVATION of TURN GOVERNING EQUATIONS:

The turn governing equations are derived from Figure A-1. The linear velocity of the point p is written in terms of the vehicle's turning radius and rotational velocity θ:

$$\dot{u}_p = \overline{O'P}\theta \ . \qquad (D\text{-}1)$$

The radial length, $\overline{OP}$ is written in terms of α and L:

$$\overline{O'P} = \frac{L}{\tan\alpha} \ . \qquad (D\text{-}2)$$

The velocity of the point p is written again in terms of α and $\dot{u}_Q$:

$$\dot{u}_p = \dot{u}_Q \cos\alpha \ . \qquad (D\text{-}3)$$

Solving equation D-1 for θ and substituting equations D-2 and D-3 yields:

$$\frac{d\theta}{dt} = \frac{\dot{u}_Q}{L} \sin\alpha \ . \qquad (D\text{-}4)$$

The x and y velocity equations are written in terms of $\dot{u}_p$ and θ:

$$\frac{dx}{dt} = \dot{u}_p \cos\theta \ , \qquad (D\text{-}5)$$

$$\frac{dy}{dt} = \dot{u}_p \sin\theta \ . \qquad (D\text{-}6)$$

Substituting equation D-3 into equations D-5 and D-6 yields:

$$\frac{dx}{dt} = \dot{u}_Q \cos\alpha\cos\theta \ , \qquad (D\text{-}7)$$

$$\frac{dy}{dt} = \dot{u}_Q \cos\alpha\sin\theta \ . \qquad (D\text{-}8)$$

DERIVATION of ANG and TT

The derivation of the equations for ANG and TT are developed using Figure D-1. Note the figure shows the vehicle entering a general turn with some initial ε_d and ε_θ.

The vehicle's steering wheel angle ANG is given by:

$$ANG = \tan^{-1}\left(\frac{L}{\rho}\right) \ . \qquad (D\text{-}9)$$

Write expressions for ρ:

$$\rho = \frac{\overline{O'P}}{\cos\hat{\varepsilon}_\theta} \ , \qquad (D\text{-}10)$$

and the length $\overline{M'N'}$:

$$\overline{M'N'} = \rho - \overline{O'P} \ . \qquad (D\text{-}11)$$

Solving equation D-10 for $\overline{O'P}$ and substituting into equation D-11 yields an expression for ρ in terms of $\overline{M'N'}$ and $\hat{\varepsilon}_\theta$:

$$\rho = \frac{\overline{M'N'}}{(1-\cos\hat{\varepsilon}_\theta)} \ . \qquad (D\text{-}12)$$

The quantity $\overline{M'N'}$ can be rewritten in terms $\hat{\varepsilon}_d$, and the distance traveled perpendicular to the next path segment in the time τ_D:

$$\overline{M'N'} = \hat{\varepsilon}_d - \dot{u}_p \tau_D \sin\hat{\varepsilon}_\theta \ . \qquad (D\text{-}13)$$

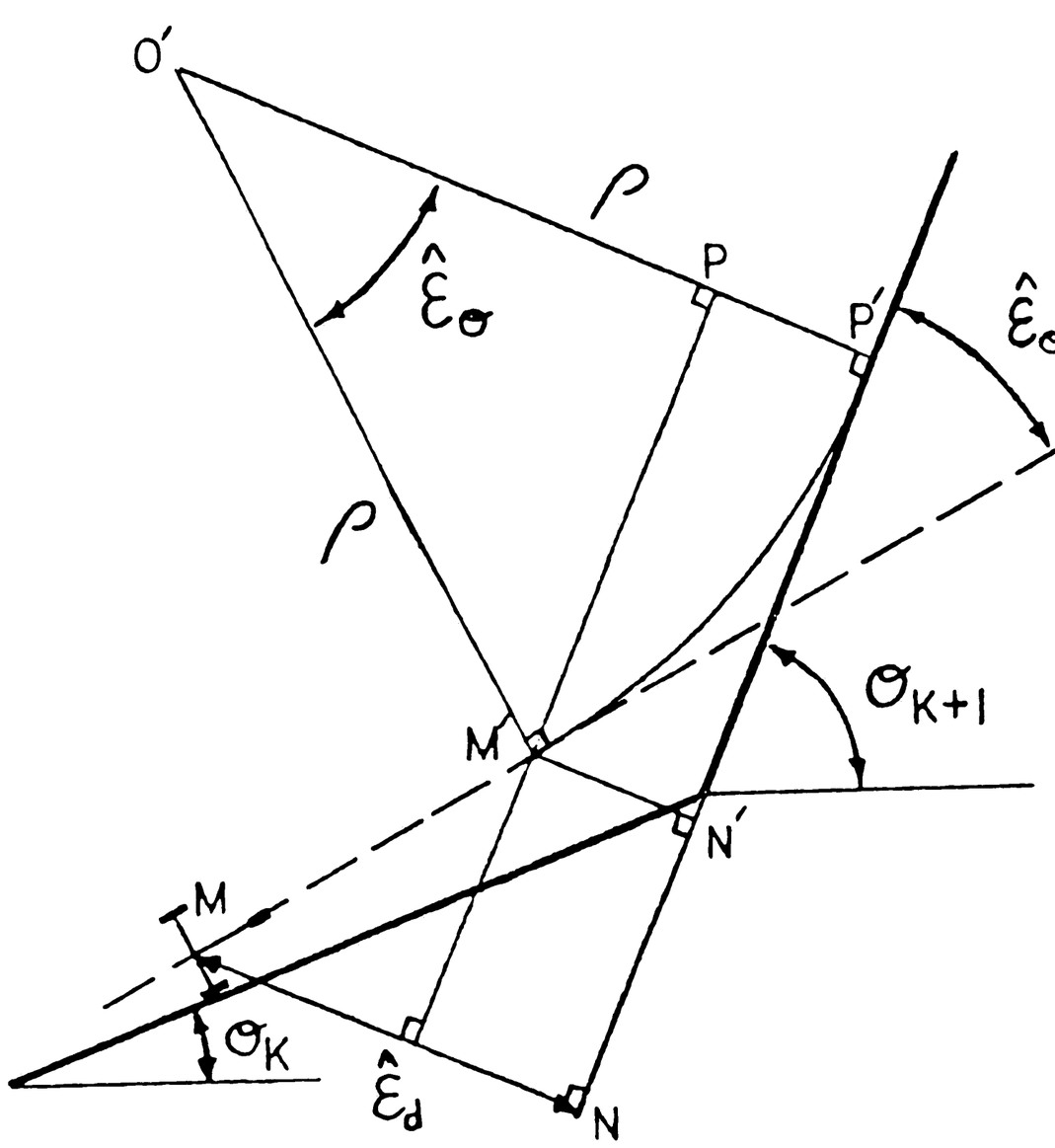

Figure D-1: Vehicle entering a general turn

Substituting equation D-13 into equation D-12, and substituting the resulting equation into equation D-9, yields:

$$ANG = \tan^{-1}\left[\frac{L(1-\cos\hat{\varepsilon}_\theta)}{\hat{\varepsilon}_d - \dot{u}_p \tau_D \sin\hat{\varepsilon}_\theta}\right] . \qquad (D\text{-}14)$$

The equation for TT is developed by realizing that the time required for the point p to travel the turn is the arc length distance divided by the velocity of point p. The arc length distance is given by:

$$\text{ARC LENGTH} = \rho\hat{\varepsilon}_\theta . \qquad (D\text{-}15)$$

TT is then written:

$$TT = \frac{\rho\hat{\varepsilon}_\theta}{\dot{u}_p} . \qquad (D\text{-}16)$$

Using equations D-12 and D-13, equation D-16 becomes:

$$TT = \frac{\hat{\varepsilon}_\theta(\hat{\varepsilon}_d - \dot{u}_p \theta_D \sin\hat{\varepsilon}_\theta)}{\dot{u}_p(1-\cos\hat{\varepsilon}_\theta)} . \qquad (D\text{-}17)$$

STEERING MODEL

The steering model represents the steering wheel angle α as a linear function of time. During a turn the steering wheel is ramped to ANG, held constant, and ramped back to zero. A diagram of α as a function of time is given in Figure D-2.

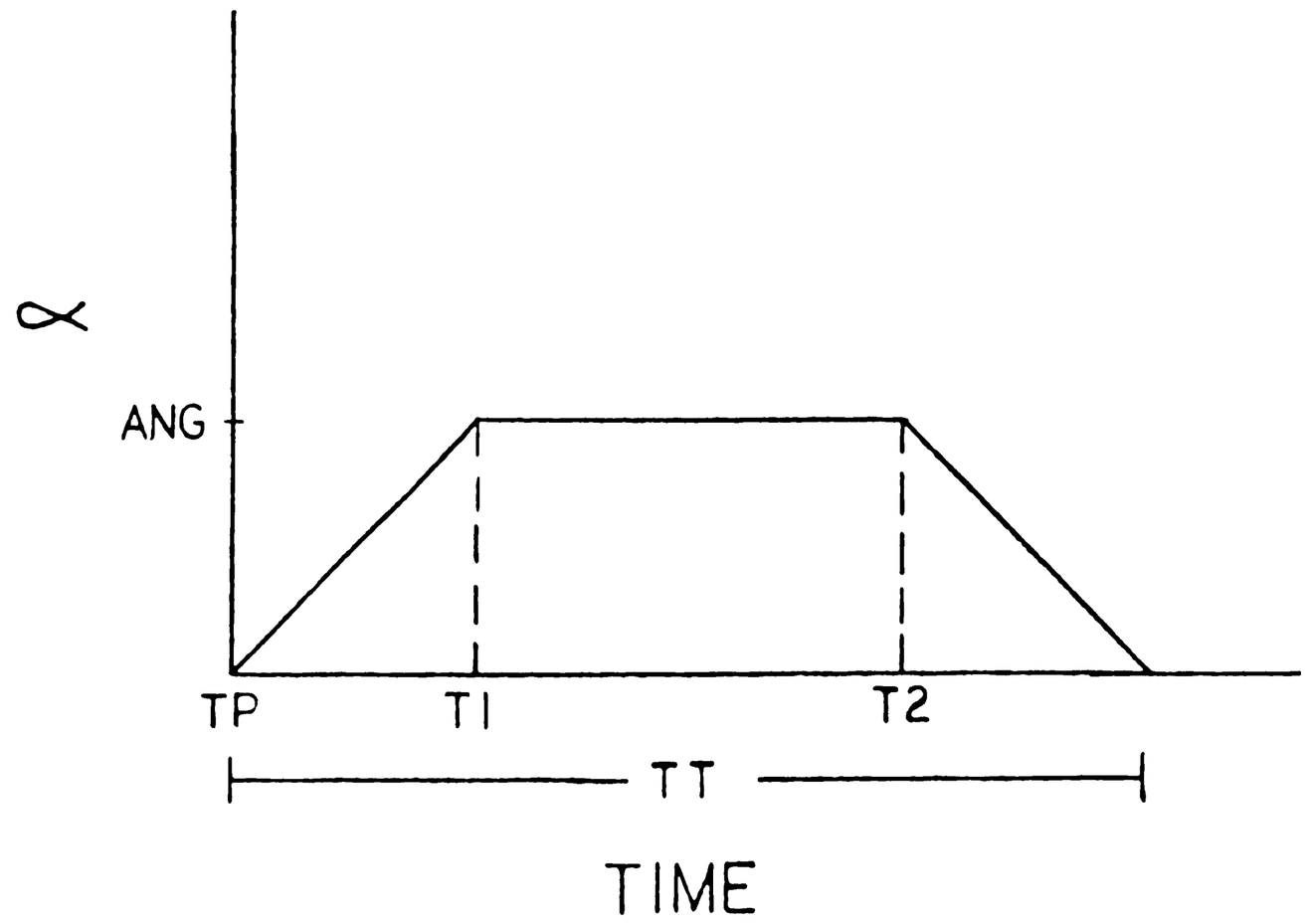

Figure D-2: Steering model

The time TP is the time at which the vehicle begins to turn. The time T1 is the time at which the steering assembly has reached ANG. The time T2 is the time at which the steering assembly begins to ramp back to zero, and is given by:

$$T2 = TT-T1 \ . \qquad (\ D\text{-}18\ )$$

APPENDIX E: VEHICLE DYNAMICS

The equations which determine the unknown forces $S_\ell+S_r$, S_f, and T are determined using Figure 4. Summing the forces on the vehicle in the x direction with x positive to the right yields:

$$T\cos_\alpha - S_f\cos\alpha = R_{r\ell}+R_{rr}+R_{rf}\cos\alpha - C\sin\beta \ . \qquad (E\text{-}1)$$

Summing the forces on the vehicle in the y direction with y positive upward yields:

$$T\sin_\alpha + S_f\sin\alpha = R_{rf}\sin\alpha + C\cos\beta - (S_\ell+S_r) \ . \qquad (E\text{-}2)$$

Summing the moments about the vehicle point Q, with the clockwise direction positive yields:

$$(S_\ell+S_r) = (1-a)C\cos\beta + \frac{E}{2L}(R_{rr}-R_{r\ell}) \ . \qquad (E\text{-}3)$$

Solving equation E-1 for $T-S_f$ gives:

$$T-S_f = R_{rf} + \frac{R_{r\ell}+R_{rr}-C\sin\beta}{\cos\alpha} \ . \qquad (E\text{-}4)$$

Solving equation E-2 for $T+S_f$ gives:

$$T+S_f = R_{rf} + \frac{aC\cos\beta + \frac{E}{2L}(R_{rr}-R_{r\ell})}{\sin\alpha} \ . \qquad (E\text{-}5)$$

Adding equations E-4 and E-5 gives an expression for the tractive force T:

$$T = R_{rf} + \frac{(R_{r\ell}+R_{rr})-C\sin\beta}{2\cos\alpha} + \frac{aC\cos\beta + \frac{E}{2L}(R_{rr}-R_{r\ell})}{2\sin\alpha} \quad .(\text{E-6})$$

Subtracting equations E-4 and E-5 gives an expression for the side force on the front wheel S_f:

$$S_f = \frac{aC\cos\beta + \frac{E}{2L}(R_{rr}-R_{r\ell})}{2\sin\alpha} - \frac{(R_{r\ell}+R_{rr})-C\sin\beta}{2\cos\alpha} \quad . \qquad (\text{E-7})$$

Using Figure 2, two relationships between β and α are developed:

$$\sin\beta = \frac{a\tan\alpha}{\sqrt{a^2\tan^2\alpha+1}} \quad , \qquad (\text{E-8})$$

and

$$\cos\beta = \frac{1}{\sqrt{a^2\tan^2\alpha+1}} \quad . \qquad (\text{E-9})$$

Substituting equations E-8 and E-9 into equations E-3, E-6, and E-7 yields expressions for $S_\ell+S_r$, T, and S_f, in terms of α, R_{rf}, $R_{r\ell}$, R_{rr}, C, E, a, and L:

$$(S_\ell+S_r) = \frac{(1-a)C}{\sqrt{a^2\tan^2\alpha+1}} + \frac{E}{2L}(R_{rr}-R_{r\ell}) \quad , \qquad (\text{E-10})$$

$$T = R_{rf} + \frac{1}{2\cos\alpha}\left[(R_{r\ell}+R_{rr}) - \frac{aC\tan\alpha}{\sqrt{a^2\tan^2\alpha+1}}\right]$$

$$+ \frac{1}{2\sin\alpha}\left[\frac{E}{2L}(R_{rr}-R_{r\ell}) + \frac{aC}{\sqrt{a^2\tan^2\alpha+1}}\right], \qquad (E\text{-}11)$$

$$S_f = \frac{1}{2\cos\alpha}\left[\frac{aC\tan\alpha}{\sqrt{a^2\tan^2\alpha+1}} - (R_{r\ell}+R_{rr})\right] +$$

$$\frac{1}{2\sin\alpha}\left[\frac{E}{2L}(R_{rr}-R_{r\ell}) + \frac{aC}{\sqrt{a^2\tan^2\alpha+1}}\right]. \qquad (E\text{-}12)$$

Equations describing $\overline{O'CM}$, and ψ are developed using Figure 4.

From the law of sines:

$$\overline{O'P} = L\frac{\cos(\alpha-\gamma_f)}{\sin(\alpha+\gamma_p-\gamma_f)}, \qquad (E\text{-}13)$$

and

$$\overline{O'Q} = L\frac{\cos\gamma_p}{\sin(\alpha+\gamma_p-\gamma_f)}. \qquad (E\text{-}14)$$

From the law of cosines:

$$\overline{O'CM}^2 = (1-a)^2L^2 + \overline{O'Q}^2 - 2(1-a)L\overline{O'Q}\sin(\alpha-\gamma_f). \qquad (E\text{-}15)$$

Substituting equations E-13 and E-14 into equation E-15 and solving for $\overline{O'CM}$ yields:

$$\overline{O'CM} = L\left[(1-a)^2 + \frac{\cos^2\gamma_p}{\sin^2(\alpha+\gamma_p-\gamma_f)} - 2(1-a)\frac{\cos\gamma_p\sin(\alpha-\gamma_f)}{\sin(\alpha+\gamma_p-\gamma_f)}\right]^{1/2}. \qquad (E\text{-}16)$$

Using the law of sines again yields:

$$\frac{\overline{O'Q}}{\sin(180-\psi)} = \frac{\overline{O'CM}}{\sin(90-\alpha+\gamma_f)}, \qquad (E\text{-}17)$$

and

$$\frac{\overline{O'Q}}{\sin\psi} = \frac{\overline{O'CM}}{\cos(\alpha-\gamma_f)} \quad . \qquad (\text{E-18})$$

Solving equation E-18 for $\sin\psi$:

$$\sin\psi = \frac{\overline{O'Q}}{\overline{O'CM}} \cos(\alpha-\gamma_f) \quad . \qquad (\text{E-19})$$

Substituting equations E-14 and E-16 into equation E-19 and solving for ψ yields:

$$\psi = \sin^{-1}\left[\frac{\cos\gamma_p \cos(\alpha-\gamma_f)}{\sin(\alpha+\gamma_p-\gamma_f)R}\right] , \qquad (\text{E-20})$$

where R is given by,

$$R = \left[(1-a)^2 + \frac{\cos^2\gamma_p}{\sin^2(\alpha+\gamma_p-\gamma_f)} - 2(1-a)\frac{\cos\gamma_p \sin(\alpha-\gamma_f)}{\sin(\alpha+\gamma_p-\gamma_f)}\right]^{1/2} . \qquad (\text{E-21})$$

Finally, equations E-3, E-6, and E-7 can be rewritten in terms ψ using the relationship:

$$\beta = 90-\psi \quad . \qquad (\text{E-22})$$

Equations E-3, E-6, and E-7 become:

$$(S_\ell + S_r) = (1-a)C\sin\psi + \frac{E}{2L}(R_{rr}-R_{r\ell}) , \qquad (\text{E-23})$$

$$T = R_{rf} + \frac{(R_{r\ell}+R_{rr})-C\cos\psi}{2\cos\alpha} + \frac{aC\sin\psi + \frac{E}{2L}(R_{rr}-R_{r\ell})}{2\sin\alpha} , \qquad (\text{E-24})$$

$$S_f = \frac{aC\sin\psi + \frac{E}{2L}(R_{rr}-R_{r\ell})}{2\sin\alpha} - \frac{(R_{r\ell}-R_{rr})-C\cos\psi}{2\cos\alpha} \quad . \qquad (\text{E-25})$$

APPENDIX F: PROGRAM INFORMATION

Three separate programs were written to complete the research:

1. STLN: Program to simulate the vehicle's motion during straight line control.

2. TURN: Program to simulate the vehicle's motion during turn control.

3. CONN: Program to simulate the vehicle's motion during complete control.

Programs 1 and 2 were run using DSS/2, a differential system solving package. DSS/2 was written by:

Dr. W.E. Schiesser

Whitacker Lab #5

Lehigh University

Bethlehem, PA 18015 U.S.A.

Program 3 was run using a fourth order Runge-Kutta integrator. See the program CONN for the actual code. All programs were run on the CYBER 730. All programs are retained by:

Dr. Russell E. Benner

Packard Lab #19

Office 466

Dept. of M.E. & Mech.

Lehigh University

Bethlehem, PA 18015 U.S.A.

REFERENCES

[1] Groover, M.P., "AGVS Overview and Summary of 1984-1985 Projects", Lehigh University, Bethlehem, Pennsylvania, October 2, 1984.

[2] Julliere, M., Murce, L., and Perrichot, H., "A Guidance System For A Vehicle Which Has To Follow A Memorized Path", L.A.T.E.A., Institut National des Sciences Appliquees, 35043 Rennes Cedex, France.

[3] Taborek, Jaroslav J., Mechanics of Vehicles, Machine Design, Cleveland, Ohio, 1957.

[4] Julliere, M., Murce, L., and Perrichot, H., "A Guidance System A Vehicle Which Has To Follow A Memorized Path", L.A.T.E.A., Institut National des Sciences Appliquees, 35043 Rennes Cedex, France.

VITA

The author was born on June 25, 1962 to Charlotte S. and Herbert W. Conover Jr. in Princeton, New Jersey. He graduated from the Peddie School in Hightstown, New Jersey in June, 1980.

He then entered Susquehanna University in Selinsgrove, Pennsylvania in September, 1980. The author graduated Cum Laude in May, 1984 and was awarded a Bachelor of Arts Degree in Physics. He is a University Scholar, a member of the Dean's List, and Who's Who Among Students in American Universities.

He began graduate study at Lehigh University in Bethlehem, Pennsylvania in September, 1984. He will be awarded a Master of Science in Mechanical Engineering in October, 1986.

The author will begin work with The Boeing Vertol Company in Philadelphia, Pennsylvania as of September, 1986.